The Drosophila TNF receptor Grindelwald couples loss of cell polarity and neoplastic growth.

Ditte Andersen, Julien Colombani, Valentina Palmerini, Krittalak Chakrabandhu, Emilie Boone, Michael Röthlisberger, Janine Toggweiler, Konrad Basler, Marina Mapelli, Anne-Odile Hueber, et al.

The Drosophila TNF receptor Grindelwald couples loss of cell polarity and neoplastic growth

Ditte S. Andersen[1,2,3,4]*, Julien Colombani[1,2,3,4]*, Valentina Palmerini[5], Krittalak Chakrabandhu[1,2,3,6], Emilie Boone[1,2,3,4], Michael Röthlisberger[7], Janine Toggweiler[7], Konrad Basler[7], Marina Mapelli[5], Anne-Odile Hueber[1,2,3,6] & Pierre Léopold[1,2,3,4]

Disruption of epithelial polarity is a key event in the acquisition of neoplastic growth. JNK signalling is known to play an important part in driving the malignant progression of many epithelial tumours, although the link between loss of polarity and JNK signalling remains elusive. In a *Drosophila* genome-wide genetic screen designed to identify molecules implicated in neoplastic growth[1], we identified *grindelwald* (*grnd*), a gene encoding a transmembrane protein with homology to members of the tumour necrosis factor receptor (TNFR) superfamily. Here we show that Grnd mediates the pro-apoptotic functions of Eiger (Egr), the unique *Drosophila* TNF, and that overexpression of an active form of Grnd lacking the extracellular domain is sufficient to activate JNK signalling *in vivo*. Grnd also promotes the invasiveness of $Ras^{V12}/scrib^{-/-}$ tumours through Egr-dependent Matrix metalloprotease-1 (Mmp1) expression. Grnd localizes to the subapical membrane domain with the cell polarity determinant Crumbs (Crb) and couples Crb-induced loss of polarity with JNK activation and neoplastic growth through physical interaction with Veli (also known as Lin-7). Therefore, Grnd represents the first example of a TNFR that integrates signals from both Egr and apical polarity determinants to induce JNK-dependent cell death or tumour growth.

We recently carried out a genome-wide screen to identify molecules that are required for neoplastic growth[1]. The condition used for this screen was the disc-specific knockdown of *avalanche* (*rotund* (*rn*)>*avl*-RNAi; *avalanche* also known as *syntaxin 7*), a gene encoding a syntaxin that functions in the early step of endocytosis[2]. *rn*>*avl*-RNAi results in ectopic Wingless (Wg) expression, neoplastic disc overgrowth[2] (Fig. 1a, b), and a 2-day delay in larva-to-pupa transition[1]. We screened a collection of 10,100 transgenic RNA interference (RNAi) lines for their ability to rescue the pupariation delay and identified 121 candidate genes[1]. Interestingly, only eight candidate genes also rescued ectopic Wg expression and neoplastic overgrowth (Extended Data Fig. 1a). These included five lines targeting core components of the JNK pathway (Bendless, Tab2, Tak1, Hemipterous and Basket; Extended Data Fig. 1b). Using a *puckered* enhancer trap (*puc-lacZ*) as a readout for JNK activity, we confirmed that JNK signalling is highly upregulated in *rn*>*avl*-RNAi discs (Fig. 1a, b, right). One of the remaining lines targets *CG10176*, a gene encoding a transmembrane protein. Reducing expression of *CG10176* by using two different RNAi lines was as efficient as *tak1* silencing to restore normal Wg pattern and suppresses JNK signalling and neoplastic growth in the *rn*>*avl*-RNAi background (Fig. 1c, d and Extended Data Fig. 1c–e). Sequence analysis of *GC10176* identified a cysteine-rich domain (CRD) in the extracellular part with homology to vertebrate TNFRs (Fig. 1e and Extended Data Fig. 2) harbouring a glycosphingolipid-binding motif (GBM) characteristic of many TNFRs including Fas[3] (Fig. 1e and Extended Data Fig. 2). We named *CG10176 grindelwald* (*grnd*), after a village at the foot of Eiger, a Swiss mountain that lent its name to the unique *Drosophila* TNF, Egr. Immunostaining and subcellular fractionation of disc extracts confirmed that Grnd localizes to the membrane (Extended Data Fig. 1f–h). Moreover, co-immunoprecipitation experiments showed that both Grnd full-length and Grnd-intra, a form lacking its extracellular domain, directly associate with Traf2, the most upstream component of the JNK pathway (Fig. 1f–h). This interaction is disrupted by a single amino acid substitution within a conserved Traf6-binding motif[4] (human TRAF6 is the closest homologue to Traf2; Fig. 1f–h and Extended Data Fig. 3). Overexpression of Grnd-intra, but not full-length Grnd, is sufficient to induce JNK signalling, ectopic Wg expression and apoptosis (Fig. 1i–j and Extended Data Fig. 4a–c), and Grnd-intra-induced apoptosis is efficiently suppressed in a hep^{75} (JNKK) mutant background (Extended Data Fig. 4d, e), confirming that Grnd acts upstream of the JNK signalling cascade.

The *Drosophila* TNF Egr activates JNK signalling and triggers cell death or proliferation, depending on the cellular context[5]. We therefore tested whether Grnd is required for the small-eye phenotype generated by Egr-induced apoptosis in the retinal epithelium[6,7] (*GMR*>*egr*; Fig. 2a, b). As previously shown, inhibition of JNK signalling by reducing *tak1* (ref. 6) or *traf2* (ref. 8) expression, or by overexpressing *puckered*[7], blocks Egr-induced apoptosis and rescues the small-eye phenotype (Extended Data Fig. 5a–d). In contrast to a previous report[9], RNAi silencing of *wengen* (*wgn*), a gene encoding a presumptive receptor for Egr, does not rescue the small-eye phenotype (Extended Data Fig. 5e). Furthermore, the small-eye phenotype is not modified in a *wgn*-null mutant background (Fig. 2c and Extended Data Fig. 5h, m, n), confirming that Wgn is not required for Egr-induced apoptosis in the eye. By contrast, reducing *grnd* levels partially rescues the Egr-induced small-eye phenotype, producing a 'hanging-eye' phenotype (Fig. 2d) that is not further rescued in a *wgn*-knockout (wgn^{KO}) mutant background (Extended Data Fig. 5e–i). A similar phenotype was previously reported as a result of non-autonomous cell death induced by a diffusible form of Egr[10] (Extended Data Fig. 5k, l). This suggests that Grnd prevents Egr from diffusing outside of its expression domain. Co-immunoprecipitation experiments show that both full-length Grnd and Grnd-extra, a truncated form of Grnd lacking the cytoplasmic domain, associate with Egr through its TNF-homology domain (Fig. 2j, k). Although Grnd-extra can bind Egr, it cannot activate JNK signalling. Therefore, we reasoned that Grnd-extra expression might prevent both cell-autonomous and non-autonomous apoptosis by trapping Egr and preventing its diffusion and binding to endogenous Grnd. Indeed, *GMR*-Gal4-mediated expression of *grnd-extra* fully rescues the Egr small-eye phenotype (Fig. 2e and Extended Data Fig. 5j). To confirm that the removal of Grnd induces Egr-mediated non-autonomous cell death, we generated wing disc

[1]University of Nice-Sophia Antipolis, Institute of Biology Valrose, Parc Valrose, 06108 Nice, France. [2]CNRS, Institute of Biology Valrose, Parc Valrose, 06108 Nice, France. [3]INSERM, Institute of Biology Valrose, Parc Valrose, 06108 Nice, France. [4]Genetics and Physiology of Growth laboratory, Institute of Biology Valrose, Parc Valrose, 06108 Nice, France. [5]Department of Experimental Oncology, European Institute of Oncology, Via Adamello 16, 20139 Milan, Italy. [6]Death receptors Signalling and Cancer Therapy laboratory, Institute of Biology Valrose, Parc Valrose, 06108 Nice, France. [7]Institute of Molecular Life Sciences, University of Zurich, Winterthurerstrasse 190, 8057 Zurich, Switzerland.
*These authors contributed equally to this work.

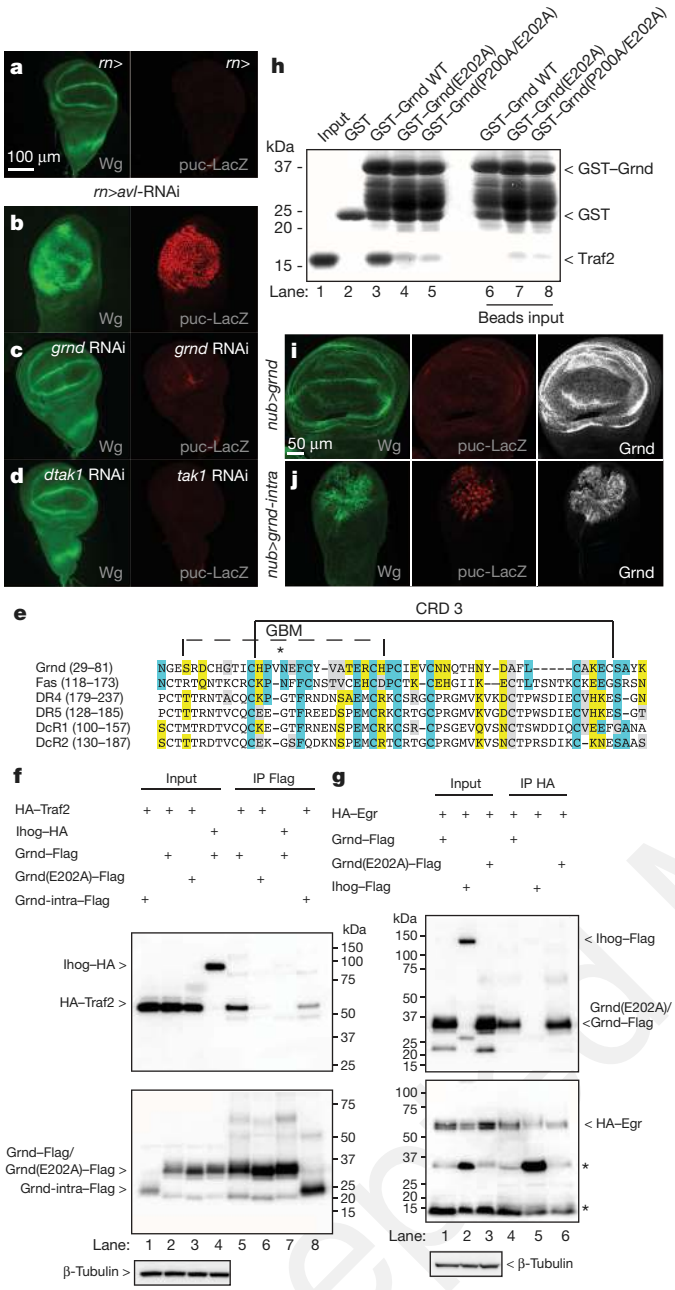

Figure 1 | Grnd is a novel member of the TNFR superfamily. a–d, Wing discs stained for Wg (left) or LacZ (right). **e**, Sequence alignment of Grnd and human TNFRs. Blue, identity; yellow, strong similarity to Grnd; grey, weak similarity to Grnd. **f**, **g**, Co-immunoprecipitation experiments from S2R^{+} cells co-expressing haemagglutinin (HA)–Traf2 or Ihog–HA (control), and either Grnd–Flag, Grnd-intra–Flag or Grnd(E202A)–Flag (**f**), or HA–Egr and either Grnd–Flag, Grnd(E202A)–Flag or Ihog–Flag (control) (**g**). Input loading is quantified using β-tubulin. **h**, Pull-down experiments of Traf2 with various truncated forms of glutathione *S*-transferase (GST)–Grnd. Commassie blue staining is used to visualize the bound species. WT, wild type. **i–j,** Wing discs stained for Wg (left), LacZ (middle) and Grnd (right).

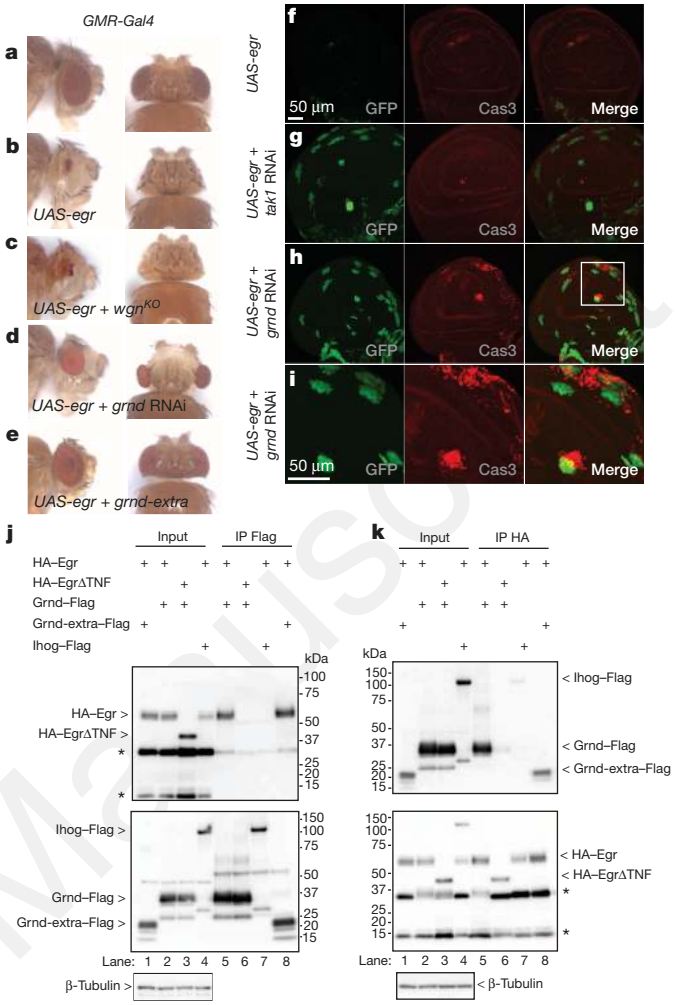

Figure 2 | Grnd is required for Egr-induced apoptosis. a–e, Light micrographs of *Drosophila* adult eyes of the indicated genotypes (all animals carry the *GMR-Gal4* driver). Original magnification, ×30. **f–i**, Wing discs carrying green fluorescent protein (GFP)-labelled clones (green) expressing *egr* (**f**), *egr* + *tak1* RNAi (**g**) or *egr* + *grnd* RNAi (**h**, **i**) and stained for Caspase 3 (Cas3; red). A close-up shows non-autonomous cell death around the *egr* + *grnd* RNAi clones. **j**, **k**, Co-immunoprecipitation (IP) experiments from S2R^{+} cells expressing HA–Egr or HA–EgrΔTNF (Egr lacking its TNF-homology domain; amino acids 278–415) and either Grnd–Flag, Grnd-extra–Flag or Ihog–Flag (control). Input loading is quantified using β-tubulin.

clones expressing *egr* alone, *egr* + *tak1* RNAi, or *egr* + *grnd* RNAi (Fig. 2f–i). As expected, reducing *tak1* levels in *egr*-expressing clones prevents their elimination by apoptosis (Fig. 2f, g). Similarly, reducing *grnd* levels prevents autonomous cell death, but also induces non-autonomous apoptosis (Fig. 2h, i). This suggests that Egr, like its mammalian counterpart TNF-α, can be processed into a diffusible form *in vivo* whose interaction with Grnd limits the potential to act at a distance. Flies carrying homozygous ($grnd^{Minos/Minos}$) or transheterozygous ($grnd^{Minos/Df}$) combinations of a transposon inserted in the *grnd* locus express no detectable levels of Grnd protein (Extended Data Fig. 6a, b) and are equally resistant to Egr-induced cell death (Extended Data Fig. 6e–j). In addition, $grnd^{Minos/Minos}$ mutant flies are viable and display no obvious phenotype (Extended Data Fig. 6c, d), suggesting that Grnd, like Egr, participates in a stress response to limit organismal damage. Collectively, our data demonstrate that Grnd is a new *Drosophila* TNF receptor that mediates most, if not all, Egr-induced apoptosis.

TNFs probably represent a danger signal produced in response to tissue damage to rid the organism of premalignant tissue or to facilitate wound healing. Disc clones mutant for the polarity gene *scribbled* (*scrib*) induce an Egr-dependent response resulting in the elimination of *scrib* mutant cells by JNK-mediated apoptosis[11,12]. To test the requirement for Grnd in this process, we compared *scrib*-RNAi and *scrib*-RNAi + *grnd*-RNAi clones obtained 72 h after heat shock induction. As expected, *scrib*-RNAi cells undergo apoptosis and detach from

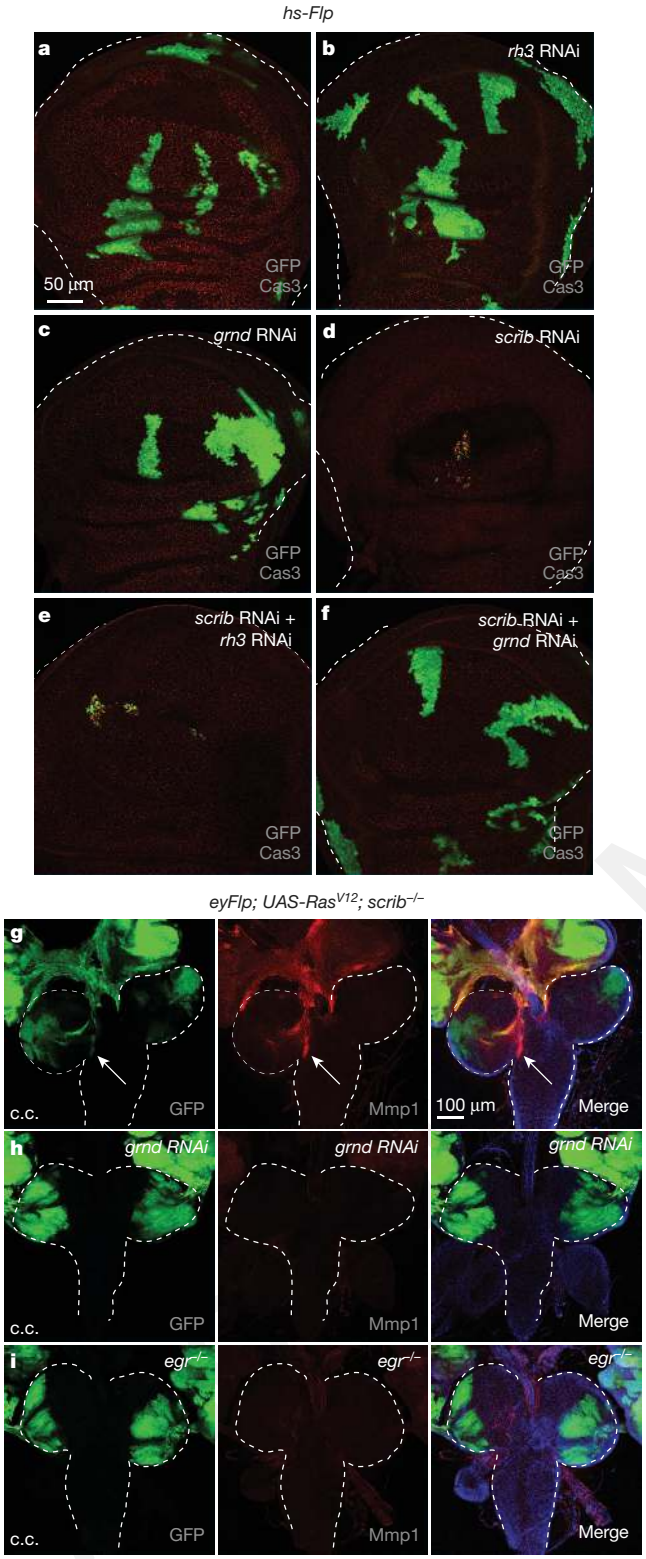

Figure 3 | Grnd is required for the Egr-induced invasiveness of *Ras^{V12}/scrib$^{-/-}$* tumours. **a–f**, Wing discs dissected 5 days after egg deposition (AED) stained for Cas3 (red) and carrying GFP-labelled clones (green) of the indicated genotypes induced 2 days AED. **a**, **b**, **e**, Wild-type clones (**a**) and clones expressing the control *Rh3* RNAi (**b**) to exclude a Gal4 titration effect (**e**). **g–i,** Eye–brain complexes dissected 7 days AED carrying *Ras^{V12}/scrib$^{-/-}$* (**g**) or *Ras^{V12}/scrib$^{-/-}$* + *grnd* RNAi (**h**) clones (labelled by GFP), or *Ras^{V12}/scrib$^{-/-}$* GFP-labelled clones in an *egr* mutant background (**i**) stained for Mmp1 (**g–i**, middle, red) and 4′,6-diamidino-2-phenylindole (DAPI; blue). *Ras^{V12}/scrib$^{-/-}$* clones invade the ventral nerve cord (**g**, white arrow). c.c., cephalic complex.

the epithelium (Fig. 3a–d). By contrast, *scrib*-RNAi clones with reduced *grnd* expression survive (Fig. 3e, f), indicating that Grnd is required for Egr-dependent elimination of *scrib*-RNAi cells. Similar results were obtained by generating *scrib$^{-/-}$* mutant clones in the eye disc (Extended Data Fig. 7a–d).

In both mammals and flies, TNFs are double-edged swords that also have the capacity to promote tumorigenesis in specific cellular contexts[5]. Indeed, *scrib$^{-/-}$* eye disc cells expressing an activated form of *Ras* (*Ras^{V12}*) exhibit a dramatic tumour-like overgrowth and metastatic behaviour, a process that critically relies on Egr[13]. *Ras^{V12}/scrib$^{-/-}$* metastatic cells show a strong accumulation of Grnd and Mmp1, and invade the ventral nerve cord[11,14,15] (Fig. 3g and Extended Data Figs 7e, 8a). Primary tumour cells reach peripheral tissues such as the fat body and the gut, where they form micrometastases expressing high levels of Grnd (Extended Data Fig. 7f, g). Reducing *grnd* levels in *Ras^{V12}/scrib$^{-/-}$* clones is sufficient to restore normal levels of Mmp1 and abolish invasiveness in a way similar to that observed in an *egr$^{-/-}$* background[13] (Fig. 3h, i and Extended Data Fig. 8a–c). Therefore, Grnd is required for the Egr-induced metastatic behaviour of *Ras^{V12}/scrib$^{-/-}$* tumorous cells. Similarly, reducing *grnd*, but not *wgn* levels, strongly suppresses Mmp1 expression in *Ras^{V12}/dlg*-RNAi cells and limits tumour invasion (Extended Data Fig. 8d–g), indicating that Wgn does not have a major role in the progression of these tumours.

Perturbation of cell polarity is an early hallmark of tumour progression in epithelial cells. In contrast to small patches of polarity-deficient cells, for example, *scrib$^{-/-}$* clones, organ compartments or animals fully composed of polarity-deficient cells become refractory to Egr-induced cell death and develop epithelial tumours. The formation of these tumours requires JNK/MAPK signalling, but not Egr[13,16], suggesting Egr-independent coupling between loss of polarity and JNK/MAPK-dependent tumour growth. In line with these observations, we noticed that, in contrast to Grnd, Egr is not required to drive neoplastic growth in *rn>avl*-RNAi conditions (Extended Data Fig. 9a, b). This suggests that, in addition to its role in promoting Egr-dependent functions, Grnd couples loss of polarity with JNK-dependent growth independently of Egr. Disc immunostainings revealed that Grnd co-localizes with the apical determinant Crb in the marginal zone, apical to the adherens junction protein E-cadherin (E-cad) and the atypical protein kinase C (aPKC; Fig. 4a and Extended Data Fig. 9c, d). In *avl*-RNAi discs, Grnd and Crb accumulate in a wider apical domain[2] (Extended Data Fig. 9e, g). Apical accumulation of Crb is proposed to be partly responsible for the neoplastic growth induced by *avl* knockdown, since overexpression of Crb or a membrane-bound cytoplasmic tail of Crb (Crb-intra) mimics the *avl*-RNAi phenotype[2] (Extended Data Fig. 9f). We therefore examined whether Grnd might couple the activity of the Crb complex with JNK-mediated neoplastic growth. Indeed, reducing *grnd* levels, but not *wgn*, in *rn>crb-intra* discs suppresses neoplastic growth as efficiently as inhibiting the activity of the JNK pathway (Fig. 4c–f and Extended Data Fig. 9h, i). Notably, Yki activation is not rescued in these conditions (Extended Data Fig. 9j–l), illustrating the ability of Crb-intra to promote growth independently of Grnd by inhibiting Hippo signalling through its FERM-binding motif (FBM)[17,18]. Indeed, neoplastic growth and polarity defects induced by a form of Crb-intra lacking its FBM (CrbΔFBM-intra) are both rescued by Grnd silencing (Fig. 4i, j). As expected, the size of *rn>crbΔFBM-intra;grnd*-RNAi discs is reduced compared to the size of *rn>crb-intra; grnd*-RNAi discs (compare Fig. 4e, f with Fig. 4j).

Crb, Stardust (Sdt; PALS1 in humans), and Pals1-associated tight junction protein (Patj) make up the core Crb complex[19], which recruits the adaptor protein Veli (MALS1–3 in humans)[20–22]. In agreement with previous yeast two-hybrid data[23], we find that Grnd binds directly and specifically to the PDZ domain of Veli through a membrane-proximal stretch of 28 amino acids in its intracellular domain (Extended Data Fig. 10a–e). Grnd localization is unaffected in

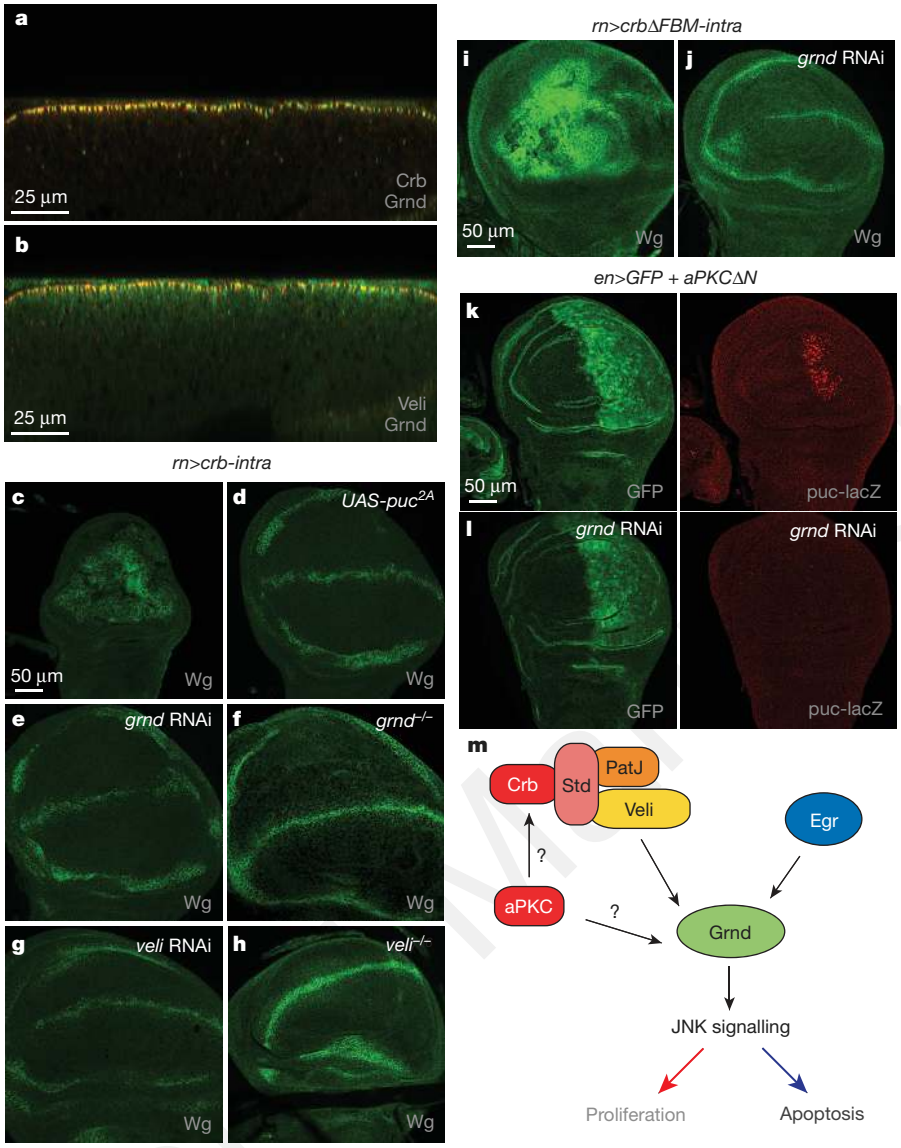

Figure 4 | *grnd* is required downstream of the apical Crb polarity complex for JNK-dependent neoplastic growth. **a, b**, Transverse sections of wild-type discs stained for Grnd (red), Crb (**a**, green) or Veli (**b**, green). **c–h**, Discs expressing *crb-intra* alone (**c**), or combined with the indicated genotypes (**d–h**), dissected 6 days AED, stained for Wg (green). **i**, **j**, Discs expressing Crb-intra lacking its FBM (*crbΔFBM-intra*) alone (**i**) or with *grnd* RNAi (**j**) stained for Wg (in green). **k**, **l**, Discs from *puc-LacZ* animals expressing activated aPKC (aPKCΔN)[26] in the posterior domain alone (**k**) or together with *grnd* RNAi (**l**). **m**, A model for Grnd function.

$crb^{-/-}$ and *veli* RNAi mutant clones (Extended Data Fig. 10f–h). However, reducing *veli* expression rescues the patterning defects and disc morphology of *rn>crb-intra* mutant cells (Fig. 4g, h), suggesting that Grnd couples Crb activity with JNK signalling through its interaction with Veli. Interestingly, aPKC-dependent activation of JNK signalling[16] also depends on Grnd (Fig. 4k, l). aPKC is capable of directly binding and phosphorylating Crb, which is important for Crb function[24]. This suggests that aPKC, either directly or through Crb phosphorylation, activates Grnd-dependent JNK signalling in response to perturbation of apico-basal polarity.

Our data are consistent with a model whereby Grnd integrates signals from Egr, the unique fly TNF, and apical polarity determinants to induce JNK-dependent neoplastic growth or apoptosis in a context-dependent manner (Fig. 4m). Recent work reveals a correlation between mammalian Crb3 expression and tumorigenic potential in mouse kidney epithelial cells[25]. The conserved nature of the Grnd receptor suggests that specific TNFRs might carry out similar functions in vertebrates, in which the link between apical cell polarity and tumour progression remains elusive.

Online Content Methods, along with any additional Extended Data display items and Source Data, are available in the online version of the paper; references unique to these sections appear only in the online paper.

Received 25 September 2013; accepted 9 February 2015.
Published online 15 April 2015.

1. Colombani, J., Andersen, D. S. & Leopold, P. Secreted peptide Dilp8 coordinates *Drosophila* tissue growth with developmental timing. *Science* **336,** 582–585 (2012).
2. Lu, H. & Bilder, D. Endocytic control of epithelial polarity and proliferation in *Drosophila*. *Nature Cell Biol.* **7,** 1232–1239 (2005).
3. Chakrabandhu, K. *et al.* The extracellular glycosphingolipid-binding motif of Fas defines its internalization route, mode and outcome of signals upon activation by ligand. *Cell Death Differ.* **15,** 1824–1837 (2008).
4. Ye, H. *et al.* Distinct molecular mechanism for initiating TRAF6 signalling. *Nature* **418,** 443–447 (2002).
5. Vidal, M. The dark side of fly TNF: an ancient developmental proof reading mechanism turned into tumor promoter. *Cell Cycle* **9,** 3851–3856 (2010).
6. Igaki, T. *et al.* Eiger, a TNF superfamily ligand that triggers the *Drosophila* JNK pathway. *EMBO J.* **21,** 3009–3018 (2002).

7. Moreno, E., Yan, M. & Basler, K. Evolution of TNF signaling mechanisms: JNK-dependent apoptosis triggered by Eiger, the *Drosophila* homolog of the TNF superfamily. *Curr. Biol.* **12,** 1263–1268 (2002).
8. Xue, L. *et al.* Tumor suppressor CYLD regulates JNK-induced cell death in *Drosophila*. *Dev. Cell* **13,** 446–454 (2007).
9. Kanda, H., Igaki, T., Kanuka, H., Yagi, T. & Miura, M. Wengen, a member of the *Drosophila* tumor necrosis factor receptor superfamily, is required for Eiger signaling. *J. Biol. Chem.* **277,** 28372–28375 (2002).
10. Narasimamurthy, R. *et al.* Structure–function analysis of Eiger, the *Drosophila* TNF homolog. *Cell Res.* **19,** 392–394 (2009).
11. Brumby, A. M. & Richardson, H. E. *scribble* mutants cooperate with oncogenic Ras or Notch to cause neoplastic overgrowth in *Drosophila*. *EMBO J.* **22,** 5769–5779 (2003).
12. Igaki, T., Pastor-Pareja, J. C., Aonuma, H., Miura, M. & Xu, T. Intrinsic tumor suppression and epithelial maintenance by endocytic activation of Eiger/TNF signaling in *Drosophila*. *Dev. Cell* **16,** 458–465 (2009).
13. Cordero, J. B. *et al.* Oncogenic Ras diverts a host TNF tumor suppressor activity into tumor promoter. *Dev. Cell* **18,** 999–1011 (2010).
14. Pagliarini, R. A. & Xu, T. A genetic screen in *Drosophila* for metastatic behavior. *Science* **302,** 1227–1231 (2003).
15. Uhlirova, M. & Bohmann, D. JNK- and Fos-regulated Mmp1 expression cooperates with Ras to induce invasive tumors in *Drosophila*. *EMBO J.* **25,** 5294–5304 (2006).
16. Sun, G. & Irvine, K. D. Regulation of Hippo signaling by Jun kinase signaling during compensatory cell proliferation and regeneration, and in neoplastic tumors. *Dev. Biol.* **350,** 139–151 (2011).
17. Ling, C. *et al.* The apical transmembrane protein Crumbs functions as a tumor suppressor that regulates Hippo signaling by binding to Expanded. *Proc. Natl Acad. Sci. USA* **107,** 10532–10537 (2010).
18. Robinson, B. S., Huang, J., Hong, Y. & Moberg, K. H. Crumbs regulates Salvador/Warts/Hippo signaling in *Drosophila* via the FERM-domain protein Expanded. *Curr. Biol.* **20,** 582–590 (2010).
19. Bulgakova, N. A. & Knust, E. The Crumbs complex: from epithelial-cell polarity to retinal degeneration. *J. Cell Sci.* **122,** 2587–2596 (2009).
20. Bachmann, A., Grawe, F., Johnson, K. & Knust, E. *Drosophila* Lin-7 is a component of the Crumbs complex in epithelia and photoreceptor cells and prevents light-induced retinal degeneration. *Eur. J. Cell Biol.* **87,** 123–136 (2008).
21. Bachmann, A. *et al.* Cell type-specific recruitment of *Drosophila* Lin-7 to distinct MAGUK-based protein complexes defines novel roles for Sdt and Dlg-S97. *J. Cell Sci.* **117,** 1899–1909 (2004).
22. Olsen, O. *et al.* Renal defects associated with improper polarization of the CRB and DLG polarity complexes in MALS-3 knockout mice. *J. Cell Biol.* **179,** 151–164 (2007).
23. Giot, L. *et al.* A protein interaction map of *Drosophila melanogaster*. *Science* **302,** 1727–1736 (2003).
24. Sotillos, S., Diaz-Meco, M. T., Caminero, E., Moscat, J. & Campuzano, S. DaPKC-dependent phosphorylation of Crumbs is required for epithelial cell polarity in *Drosophila*. *J. Cell Biol.* **166,** 549–557 (2004).
25. Karp, C. M. *et al.* Role of the polarity determinant crumbs in suppressing mammalian epithelial tumor progression. *Cancer Res.* **68,** 4105–4115 (2008).
26. Betschinger, J., Mechtler, K. & Knoblich, J. A. The Par complex directs asymmetric cell division by phosphorylating the cytoskeletal protein Lgl. *Nature* **422,** 326–330 (2003).

Acknowledgements We thank G. Jarretou for technical assistance, the Vienna *Drosophila* RNAi Centers, the *Drosophila* Genetics Resource Center, the Bloomington Stock Center, N. Caridi and S. Pasqualato for technical assistance and P.L. laboratory members for comments on the manuscript. This work was supported by the CNRS, INSERM, Agence Nationale de la Recherche, Fondation pour la Recherche Médicale, Association pour la Recherche contre le Cancer (grant no. PJA20131200042 to J.C.), European Research Council (Advanced grant no. 268813 to P.L.), Marie Curie Life Long Training (grant no. 252373 to D.S.A.), the Labex Signalife program (grant ANR-11-LABX-0028-01 to P.L.), the Italian Association for Cancer Research (AIRC IG-12877) and the Italian Ministry of Health (GR-2008-1134103) to M.M.

Author Contributions D.S.A., J.C., K.C., A.-O.H., K.B., M.M. and P.L. designed the research; D.S.A., J.C., K.C., V.P., E.B., M.R. and J.T. performed experiments; D.S.A., J.C., K.C., E.B., A.-O.H., K.B., V.P., M.M. and P.L. analysed the data; D.S.A., J.C. and P.L. wrote the manuscript.

METHODS

Fly strains and food. Animals were reared at 25 °C on fly food containing, per litre: 17 g inactivated yeast powder, 83 g corn flour, 10 g agar, 60 g white sugar and 4.6 g Nipagin M (in ethanol). The *rn*-Gal4, *UAS-egr*, *tub*GAL80^{ts} animals were raised at 18 °C, shifted to 30 °C for 40 h during early third instar larval development (7 days AEL), and subjected to dissection immediately after (Extended Data Fig. 6).

Cell culture. *Drosophila* S2 and S2R$^+$ cells were grown in complete Schneiders medium (CSM; Schneiders medium (Invitrogen) supplemented with 10% heat-inactivated FBS (BioWhittaker), 50 U ml^{-1} penicillin and 50 μg ml^{-1} streptomycin (Invitrogen)) at 25 °C. Transfections were done using Effectene reagent (Qiagen).

Plasmids. *grnd*, *grnd-extra* and *grnd-intra* coding sequences were PCR amplified from BDGP EST complementary DNA clones RE28509, and cloned into the pENTR/D-TOPO vector using the following gene-specific primers: sense primers CACCATGTCGGTCAGGAAGTTGAG (*grnd* and *grnd-extra*) and CACCA TGCTGATCCTCTTGCTGCTGACTATCC (*grnd-intra*); and antisense primers GAAAGCGACGGGAATCGTCGC (*grnd* and *grnd-intra*) and CCATCGAAGG AACTGAAACGCG (*grnd-extra*). The mutations giving rise to the single E202A and double P200A/E202A amino acid changes in Grnd and Grnd$^{125–241}$ were introduced using the QuickChange site-directed mutagenesis kit (Stratagene), *grnd-pENTR* or *grnd*$^{125–241}$*-pGEX-6PI* templates, and the following primers: sense, CGGTGAGCACTCGCTATCCGGCGGCAAACAGTACCACGCCCAC; and antisense, GTGGGCGTGGTACTGTTTGCCGCCGGATAGCGAGTGCTCAC CG for *grnd*^{E202A}; sense, CGGTGAGCACTCGCTATGCGGCGGCAAACAGT ACCACGCCCAC; and antisense, GTGGGCGTGGTACTGTTTGCCGCCGCA TAGCGAGTGCTCACCG for *grnd*$^{P200A/E202A}$. To generate *grnd-Flag*, *grnd*^{E202A}*-Flag*, *grnd-extra-Flag* and *grnd-intra-Flag*, *grnd*, *grnd*^{E202A}, *grnd-extra* and *grnd-intra* coding sequences were cloned into the Gateway Destination vector pActin-3×Flag (*Drosophila* Gateway Vector Collection) for expression in S2 and S2R$^+$ cells. In addition, *grnd*, *grnd-intra* and *grnd-extra* coding sequences were cloned into pUASg.attB for generation of UAS-*grnd*, *UAS-grnd-intra* and UAS-*grnd-extra* transgenic lines. The *HA-traf2* plasmid was from K.B.[27]. The *HA-egr* and *HA-egrΔTNF* plasmids were a gift from M. Miura. pActin-iHog-HA and pActin-iHog-Flag were gifts from L. Ruel.

Transgenic flies. To generate the *UAS-grnd UAS-grnd-intra* and *UAS-grnd-extra* lines, the *pUASattB-grnd*, *pUASattB-grnd-intra* and *pUASattB-grnd-extra* constructs were introduced into the germ line by injections in the presence of the PhiC31 integrase and inserted in the 86F8-landing site on the 3R chromosome (Bloomington *Drosophila* Stock Center, BL24749, BestGene). The following RNAi lines were from the GD or KK collections of the Vienna *Drosophila* RNAi Center (VDRC): *grnd* RNAi (GD43454, sense primer CGCGAATTCCCTCTTGCTG CTGACTATCCTTCTCGT, and antisense primer GCGTCTAGAGTTGTGG GCGTGGTACTGTTTTCC; and KK104538, sense primer TGGCGCCCCTAG ATGAACGGTTATGACGGAGATCG, and antisense primer CGCATGTAGC CTGCCGTTTGTGGTGATTGCGAATG), *tak1* RNAi (KK101357, sense primer TGGCGCCCCTAGATGGCTTGTCCTTGAAGTCCTGC, and antisense primer CGACGCCCGCTGATAGCATGAGCAGGAGATTGTCA), *bendless* RNAi (KK109638, sense primer TGGCGCCCCTAGATGCGCATCATCAAGGAGA CTCA, and antisense primer CGCATGTAGCCTGCCTTCTGGAAAAACGCC GATAC), *tab2* RNAi (KK100326, sense primer TGGCGCCCCTAGATGGCA CTTTCAGCGGAAGAAAC, and antisense primer TAGCCTCCCTAGCG CAGCTCTGCACTGGGATAGGA), *traf2* RNAi (GD16125, sense primer CGC GAATTCAGCACCCACTCCGCCCAAGA, and antisense primer GCGTCTAG AACCGAACAGCCCAGCGAGGA), *hep* RNAi (KK109277, sense primer TGG CGCCCCTAGATGGGCTTCTTGGACAGCTTGAG, and antisense primer CG CATGTAGCCTGCCAGGAGAACAAACGCATCCTG), *bsk* RNAi (KK104569, sense primer TGGCGCCCCTAGATGAGCATCCACTTCCTCAGCAT, and antisense primer TAGGTCTAGCCCCGCGGTACACCATCACCCTCGTT), *scrib* RNAi (GD 45556, sense primer CGCGAATTCCGAAGAGGACAACG CACAGCA, and antisense primer GCGTCTAGACTGGGAGCGGGCAAAGT GTAAG), *avl* (GD5413, sense primer CGCGAATTCCAACAGTAGCGCCAG CCAGCA, and antisense primer CGCTCTAGACCGTGCCCTGCGAGACA AAA), *dilp8* (KK102604, sense primer TGGCGCCCCTAGATGACTCGATG GACCTTCTGTCG, and antisense primer CGCATGTAGCCTGCCGTCATCG GAGTCTGTTGCCT), and *rh3* RNAi (KK100853, sense primer TGGCGCCCC TAGATGATCTGGGATGACTTATGGCG, and antisense primer TAGCCTCC CTAGCGCTCGATACGCGACTCTTTGTG). The *veli*-RNAi lines were from U. Thomas. The *wengen*-RNAi line (*wengen-IR*) was provided by M. Miura. The *GMR*-Gal4 (on chromosome II), *UAS-egr* (on chromosome III), GMR-Gal4, *UAS-ecto-egr60* (on chromosome II), *GMR*-Gal4, *UAS-egr* (on chromosome II), *UAS-CrbΔFBM-intra*, *DIAP-GFP*, *aPKCΔN*, *FRT*, *Crb*^{11A22} (null) and *UAS-wgn* transgenic lines were previously published[7,10,27–29], the *UAS-puc*^{2A} line was described previously[30], the *UAS-crb-intra* transgenic lines and *veli*^{66} mutant flies were from E. Knust, the *egr*^{1} and *egr*^{3} mutant lines and the UAS-ras^{V12}; FRT82B, *scrib*^{1}/TM6b and UAS-ras^{V12}, *egr*^{3}; FRT82B, scrib^{1}/TM6b and yw, eyFlp1; act>y+>Gal4, UAS-GFP; FRT82B, tubgal80 and yw, eyFlp1; act>y+>Gal4, UAS-GFP, *egr*^{1}; FRT82B, tubGal80 lines were from M. Vidal, the *w*^{1118}; +; *rn*Gal4, *UAS-eiger*, *tubGal80*^{ts}*/TM6B* line was provided by I. Hariharan, the *yw, hep75/FM7, GFP*; *Sal*^{PE}*/cyo* line was provided by F. Serras. The *rn*-Gal4, *nub*-Gal4, puc-LacZ, *grnd*^{Minos} (Mi{MIC}CG10176^{MI05292}), and *grnd*$^{Df(BSC149)}$ lines were provided by the Bloomington *Drosophila* Stock Center.

Flies' eye pictures are acquired on a Leica Fluorescence Stereomicroscope MZ16 FA with a Leica digital camera DFC 490.

Generation of *wgn*$^{KO/KO}$ mutant flies. The *wgn* knockout allele was generated by ends-in gene targeting as described previously[31]. The pTV2 targeting construct carried frameshift mutations in exon 1 and 2, an I-SceI site between these two exons, a *white*$^+$ marker gene, an I-CreI site, up- and downstream homology sequences and two flanking FRT sites. The frameshift mutations were introduced by cutting the unique intrinsic restriction sites AclI and NotI followed by T4 DNA polymerase-mediated fill-in. F3 Larvae carrying the targeting construct together with an *hsp70-flp* and a *hsp70-I-SceI* transgene were heat shocked (1 h at 38 °C on day 2 and 3 after egg laying) to generate a linearized targeting construct that aligns and recombines with the endogenous wild-type locus. After crossing the F3 flies to eye-FLP-expressing flies, the F4 was screened for non-mosaic *white*$^+$ eyed flies carrying an insertion of a processed targeting construct. After processing with FLP and I-SceI, only one FRT site remained next to the *white*$^+$ marker gene in these flies. Flies still carrying the original donor insertion lost the *white*$^+$ marker gene, since it was still flanked by two FRT sites. Female F4 '*w*$^+$ *wgn*^{KO}' flies, carrying two *wgn* copies on the X chromosome were crossed with males of the genotype 'v/Y ; +/+ ; [v+, 70I-CreI] 1A/TM6'. The F5 offspring were heat shocked (1 h at 38 °C on day 2 after egg laying). F5 offspring males were selected against TM6 ('w+/−74/Y ; +/+ ; [v+, 70I-CreI] 1A/+') and typically displayed *white*$^{+/-}$ mosaics. When they were individually crossed to the X-chromosomal balancer stock 'bin/#852', more than 90% of the males were sterile. The F6 flies that hatched were either *white*$^+$ or *white*$^-$. The *white*$^-$ flies were tested for the presence of the mutations. The stocks 'y w (v); P[ry+, 70FLP]4 P[v+, 70I-SceI]2B Sco/S2 Cyo' and 'v; +/+; [v+, 70I-CreI] 1A/ TM6, Ubx, e' were provided by K. Golic and Y. Rong.

Genome-wide screen. As an unbiased approach to identify molecules that are required for neoplastic growth, we used the *elavGal80*; *rn>avl*-RNAi/ *TM6b, tub>Gal80* testerline, which is characterized by neoplastic growth in the discs and a delay of about 2 days in pupariation. We crossed this line to the Vienna *Drosophila* RNAi Center (VDRC) collection of *phiC31* (KK) RNAi lines (10,100 lines) and screened for candidates that were able to rescue the delay at pupariation as described previously[1]. One-hundred and twenty-one candidates significantly rescued the pupariation delay in *rn>avl*-RNAi larvae. Of these, only 8 lines rescued the neoplastic disc growth (Extended Data Fig. 1)

Immunostainings of larval tissues. Tissues dissected from larvae in 1× PBS (137 mM NaCl, 2.7 mM KCl, 4.3 mM Na_2HPO_4, 1.47 mM KH_2PO_4, pH 8) at the indicated hour AED, were fixed in 4% formaldehyde (Sigma) in PBS for 20 min at room temperature washed in PBS containing 0.1% Triton X-100 (PBT), blocked for 2 h in PBT containing 10% FBS (PBS-TF), and incubated overnight with primary antibodies at 4 °C. The next day, cells and tissues were washed, blocked in PBS-TF, and incubated with secondary antibodies at 1/500 dilution (Rhodamine Red-X-conjugated donkey anti-rat, Cy3 conjugated donkey anti-rabbit, Cy3 conjugated donkey anti-chicken, Cy3 conjugated donkey anti-mouse and Cy3 conjugated mouse anti-guinea pig, Cy5 conjugated donkey anti-rat, and Cy5 conjugated donkey anti-guinea pig from Jackson ImmunoResearch, goat anti-mouse Alexa Fluor 488, donkey anti-rat Alexa Fluor 488 and goat anti-rabbit Alexa Fluor 488 from Invitrogen) for 2 h at room temperature. After washing, tissues were mounted in Vectashield containing DAPI for staining of DNA (Vector Labs). Fluorescence images were acquired using a Leica SP5 DS (×20 and ×40 objectives) and processed using Adobe Photoshop CS5.

Lysis and immunoprecipitations. Cells were lysed in 100 μl buffer A (50 mM Tris-HCl (pH 8), 150 mM NaCl, 1% NP-50, 1 mM EGTA, 0.5 M NaF, phosphatase inhibitor cocktail 2 (Sigma), complete protease inhibitor cocktail (Roche)). Immunoprecipitations were performed from about 1 × 10^7 S2 cells. Cells were lysed in 200 μl buffer A, and cell extracts were cleared of membranous material by centrifugation at 10,000 r.p.m. for 15 min. The cleared extracts were incubated with protein G-Sepharose beads (Sigma) for 1 h to reduce unspecific binding of proteins to the beads in the subsequent purifications. Next, the precleared extracts were incubated with 80 μl of protein G-Sepharose beads and 1 μl of the relevant antibody for 3 h. Subsequently, beads were washed three times in buffer A, boiled in sample and reducing buffers (Invitrogen).

Protein preparation. *Drosophila* Veli full length (Veli$^{1-195}$) and PDZ domain (Veli$^{85-195}$) were expressed with an amino-terminal His_6-tag from pET43 (Novagen) in *Escherichia coli* strain BL21 Rosetta, and purified by affinity on Ni-NTA beads (Qiagen). The Veli L27 domain (Veli$^{1-81}$) was cloned in a modified pET43 plasmid as a His_6–MBP-tagged construct. The fusion protein was expressed in bacteria similarly to the other constructs. After a first step of affinity purification on amylose beads (NEB), the protein was incubated with TEV protease (Invitrogen Life Technologies) to cleave the MBP tag, and loaded on a Resource-Q anion-exchange column (GE-Healthcare). The TRAF domain of *Drosophila* Traf2 (Traf2$^{319-475}$) was expressed similarly, and purified by affinity followed by ion-exchange chromatography on a Resource-S column (GE-Healthcare). All Grnd constructs were expressed as GST-fusion proteins using a modified version of the pGEX-6PI vector (GE-Healthcare), and purified by affinity on glutathione sepharose (GSH) beads. The purifications were carried out at 4 °C. The PDZ domains of human Par3 (Par3-PDZ2 and Par3-PDZ3 encompassing residues 465–548 and 582–685, respectively) and *Drosophila* Bazooka (Baz-PDZ1 corresponding to residues 331–419) were expressed as GST-fusion proteins. After the first step of affinity purification on GSH-beads, the GST tag was removed from the constructs by cleavage with PreScission protease, and the PDZ domains were further purified by ion-exchange chromatography.

***In vitro* binding assay.** To test the interaction properties of intracellular Grnd constructs, GST–Grnd fusion proteins (5 μM) adsorbed on GSH-beads were incubated for 40 min at 4 °C with 10 μM Veli^{FL}, Veli^{L27} or Veli^{PDZ} in a buffer containing 10 mM HEPES pH 7.4, 30 mM NaCl, 5% glycerol, 0.5 mM EDTA and 1 mM dithiothreitol (DTT). After two washing steps, the bound species were resolved on SDS–PAGE and visualized by Coomassie staining. To test the specificity of binding, analogous pull-down assays were performed with the PDZ domains of Par3 and Bazooka under the same conditions. To monitor the ability of Traf2 to bind Grnd, 2 μM GST–Grnd$^{125-241}$ wild type or mutated on P200 and/or E202 were absorbed on GSH beads and incubated with 10 μM Traf2$^{319-475}$ in a buffer consisting of 10 mM HEPES pH 7.4, 0.15 M NaCl, 5% glycerol, 0.5 mM EDTA, 1 mM DTT and 0.05% Tween. After washing, complexes immobilized on beads were analysed by SDS–PAGE.

Subcellular fractioning. Subcellular fractioning of 300 wing imaginal discs dissected from wild-type animals was performed using the Qproteome Cell Compartment Kit (Qiagen) according to the manufacturer's protocol.

Western blotting. Proteins were resolved by SDS–PAGE using 4–12% gradient gels (NuPAGE Novex gel, Invitrogen) and transferred electrophoretically to polyvinylidene difluoride membranes (Milipore). The membranes were incubated for 1 h in blocking buffer (PBS, 5% milk) and incubated overnight at 4 °C in the same buffer containing primary antibodies at 1:1,000 dilutions: rabbit anti-Smoothened[32], mouse anti-Lamin (Developmental Studies Hybridoma Bank (DSHB)), mouse anti-Dlg (4F3) from DSHB, mouse anti-Myc 9E10 (sc-40, Santa Cruz Biotechnology), rabbit anti-Myc A-14 (sc-789, Santa Cruz Biotechnology), mouse anti-Flag F3165 (Sigma), rat anti-HA 3F10 (Roche)), guinea pig anti-Grnd at 1:1,000, anti-tubulin (Sigma) at 1:2,000. The anti-Wgn antibody was used as described previously[27]. Membranes were washed three times in PBS-T, blocked for 1 h, and probed with secondary antibodies in blocking buffer for 1 h at room temperature. After three washes in PBS-T, chemiluminescence was observed using the ECL-Plus western blotting detection system (Amersham Biosciences). Images were generated using the Fujifilm Multi Gauge software.

Antibodies. To generate purified antisera specific for the Grnd protein, two peptides, CAYPHPATANGKDLNA and NAINHPGSDLERAQSQ, corresponding to amino acids 140–154 and 161–176, respectively, were used as immunogens in guinea pigs (Eurogentec). The following primary antibodies were used for immunoflourescence in this study: mouse anti-Wg (4D4) from DSHB 1/50, mouse anti-Dlg (4F3) from DSHB 1/500, rat anti-E-Cad (DCAD2) from DSHB 1/500, mouse anti-MMP1 (3A6B4/5H7B11/3B8D12; the three different antibodies were mixed in amounts (1:1:1) from DSHB (1:25)), chicken anti-β-galactosidase from GeneTek 1/1,000, rabbit anti-cleaved caspase-3 (Asp 175) from Cell Signaling Technology 1/500, rabbit anti-aPKC from Santa Cruz Biotechnology 1/1,000, guinea pig anti-Grnd 1/100, rabbit anti-Veli 1/1,000 (gift from G. Pietrini), and rat anti-Crb 1/1,000 (gift from E. Knust).

Sequence alignment and homology modelling. Multiple sequence alignment, per cent identity matrix, and phylogenic data were generated using Clustal Omega (http://www.ebi.ac.uk/Tools/services/web/toolform.ebi?tool=clustalo). Data of five human death receptors of the TNFR superfamily with the highest identity with Grnd are shown. Slight manual adjustment of the alignments was performed. Amino acids are highlighted where Grnd shares identity or similarity with death receptor(s) (Fig. 1) or Grnd-like proteins from other insect species (Extended Data Fig. 2d), or where Fas shares identity or similarity with Grnd and/or Wgn (Extended Data Fig. 2b). Amino acid similarity is presented based on scores in Gonnet PAM 250 matrix (>0.5, highly similar; ≤0.5, weakly similar). Amino acid positions are indicated in parentheses or at the end of the shown sequences. The phylogram was drawn using interactive Tree of Life[33] (http://itol.embl.de/). Number on each branch indicates branch length (Extended Data Fig. 2a). UniProt protein identifiers are: Fas (P25445), DR4 (O00220), DR5 (O14763), DcR1 (O14798), DcR2 (Q9UBN6), and Wengen (Q9VWS4). Information of protein domains in TNFR superfamily members used to construct protein domain diagram (Extended Data Fig. 2d) was obtained from UniProt (http://www.uniprot.org/).

Genotypes. Fig. 1a: w^-; +; *rn*-Gal4/ *puc-lacZ*. Fig. 1b: w^-; *elav*-Gal80/+; *rn*-Gal4, *UAS avl* RNAi GD/ *puc-lacZ*. Fig. 1c: w^-; *elav*-Gal80/ *UAS grnd* RNAi KK; *rn*-Gal4, *UAS avl* RNAi GD/*puc-lacZ*. Fig. 1d: w^-; *elav*-Gal80/ *UAS tak1* RNAi KK; *rn*-Gal4, *UAS avl* RNAi GD/*puc-lacZ*. Fig. 1i: w^-; *nub*-Gal4/+; *UAS grnd* / *puc-lacZ*. Fig. 1j: w^-; *nub*-Gal4/+; *UAS grnd-intra* / *puc-lacZ*.

Fig. 2a: w^-; *GMR*-Gal4/+; +. Fig. 2b: w^-; *GMR*-Gal4, *UAS egr*/+; MKRS/+. Fig. 2c: wgn^{KO}; *GMR*-Gal4, *UAS egr*/+; MKRS/+. Fig. 2d: w^-; *GMR*-Gal4, *UAS egr*/ UAS *grnd* RNAi KK; MKRS/+. Fig. 2e: w^-; *GMR*-Gal4, *UAS egr*/ +; MKRS/ *UAS grnd-extra*. Fig. 2f: *yw, hs-FLP; Act>CD2>*Gal4, *UAS GFP*/+; *UAS egr*/+. Fig. 2g: *yw, hs-FLP; Act>CD2>*Gal4, *UAS GFP/ UAS tak1* RNAi KK; *UAS egr*/+. Fig. 2h–i: *yw, hs-FLP; Act>CD2>*Gal4, *UAS GFP/ UAS grnd* RNAi KK; *UAS egr*/+.

Fig. 3a: *yw, hsFLP; Act>CD2>*Gal4, *UAS GFP*/+; +. Fig. 3b: *yw, hs-FLP; Act>CD2>*Gal4, *UAS GFP/ UAS rh3* RNAi KK; +. Fig. 3c: *yw, hs-FLP; Act>CD2>*Gal4, *UAS GFP/ UAS grnd* RNAi KK; +. Fig. 3d: *yw, hs-FLP; Act>CD2>*Gal4, *UAS GFP*/+; *UAS scrib* RNAi GD/+. Fig. 3e: *yw, hs-FLP; Act>CD2>*Gal4, *UAS GFP/ UAS rh3* RNAi KK; *UAS scrib* RNAi GD/+. Fig. 3f: *yw, hs-FLP; Act>CD2>*Gal4, *UAS GFP/ UAS grnd* RNAi KK; *UAS scrib* RNAi GD/+. Fig. 3g: *yw, ey-FLP*; *Act>y$^+$>*Gal4, *UAS GFP*; *UAS ras^{V12}*/+; *FRT82B, scrib^1*/ FRT82B, *tub*Gal80. Fig. 3h: *yw, ey-FLP*; *Act>y$^+$>*Gal4, *UAS GFP; UAS ras^{V12}*, UAS *grnd* RNAi KK /+; *FRT82B, scrib^1*/ FRT82B, *tub*Gal80. Fig. 3i: *yw, ey-FLP*; *Act> y$^+$>*Gal4, *UAS GFP*; *egr^1* / *UAS ras^{V12}*, *egr^3*; *FRT82B, tub*Gal80/ *FRT82B, scrib^1*.

Fig. 4a, b: w^-. Fig. 4c: w^-; *UAS crb-intra*/+; *rn*-Gal4 /+. Fig. 4d: w^-; *UAS crb-intra/ UAS puc^{2A}*; *rn*-Gal4 /+. Fig. 4e: w^-; *UAS crb-intra/ UAS grnd* RNAi KK; *rn*-Gal4 /+. Fig. 4f: w^-; *grnd^{Minos}/ grnd^{Minos}*; *rn*-Gal4 / *UAS crb-intra*. Fig. 4g: w^-; *UAS crb-intra/ UAS veli* RNAi ; *rn*-Gal4/ *UAS veli* RNAi. Fig. 4h: w^-; *UAS crb-intra/ nub*-Gal4 ; *veli^{66}*/ *veli^{66}*. Fig. 4i: w^-; +; *UAS crbΔFBM-intra/ rn*-Gal4. Fig. 4j: w^-; *UAS grnd* RNAi KK/+ ; *UAS crbΔFBM-intra/ rn*-Gal4. Fig. 4k: w^-; *en*-Gal4, *UAS GFP*/+; *UAS aPKCΔN/ puc-lacZ*. Fig. 4l: w^-; *UAS grnd* RNAi KK/ *en*-Gal4, *UAS GFP; UAS aPKCΔN/ puc-lacZ*.

Extended Data Fig. 1c: w^-; *elav*-Gal80/+; *rn*-Gal4, *UAS avl* RNAi GD /+. Extended Data Fig. 1d: w^-; *elav*-Gal80/ *UAS grnd* RNAi GD; *rn*-Gal4, *UAS avl* RNAi GD /+. Extended Data Fig. 1e: w^-; *elav*-Gal80/ *Rh3* RNAi KK; *rn*-Gal4, *UAS avl* RNAi GD /+. Extended Data Fig. 1f, g: w^-; *ptc*-Gal4, *UAS-GFP*/ UAS *grnd* RNAi KK; +.

Extended Data Fig. 4a: w^-; +; *rn*-Gal4 /+. Extended Data Fig. 4b: w^-; +; *rn*-Gal4 / *UAS grnd*. Extended Data Fig. 4c, d: w^-; +; *rn*-Gal4 / *UAS grnd-intra*. Extended Data Fig. 4e: yw^-; *sal*-Gal4 /+; *UAS grnd-intra* /+. Extended Data Fig. 4f: yw^-, *hep^{75}*; *sal*-Gal4 /+; *UAS grnd-intra* /+.

Extended Data Fig. 5a: w^-; *GMR*-Gal4, *UAS egr*/+; MKRS/+. Extended Data Fig. 5b: w^-; *GMR*-Gal4, *UAS egr*/ *UAS-traf2* RNAi GD; MKRS/+. Extended Data Fig. 5c: w^-; *GMR*-Gal4, *UAS egr*/ *UAS puc^{2A}*; MKRS/+. Extended Data Fig. 5d: w^-; *GMR*-Gal4, *UAS egr*/ UAS *tak1* RNAi KK; MKRS/+. Extended Data Fig. 5e: w^-; *GMR*-Gal4, *UAS egr*/ *UAS-wengen* RNAi IR; MKRS/+. Extended Data Fig. 5f: w^-; *GMR*-Gal4, *UAS egr*/ *UAS-grnd* RNAi GD; MKRS/+. Extended Data Fig. 5g: wgn^{KO}; *GMR*-Gal4, *UAS egr*/ *UAS-grnd* RNAi GD; MKRS/+. Extended Data Fig. 5h: wgn^{KO}; +; +. Extended Data Fig. 5i: w^-; *GMR*-Gal4/ *UAS-grnd* RNAi KK; +. Extended Data Fig. 5j: w^-; *GMR*-Gal4/+; *UAS-grnd-extra*/+. Extended Data Fig. 5k: w^-; *GMR-Gal4*, *UAS-ecto-egr60*/+; MKRS/+. Extended Data Fig. 5l: w^-; *GMR-Gal4*, *UAS-ecto-egr60*/ *UAS puc^{2A}*; MKRS/+.

Extended Data Fig. 6c: w^-. Extended Data Fig. 6d: w^-; *grnd^{Minos}/ grnd^{Minos}*; +. Extended Data Fig. 6e: w^-; +; *rn*-Gal4, *UAS egr, tub*Gal80^{ts} /+. Extended Data Fig. 6f: w^-; *UAS-grnd* RNAi KK/+; *rn*-Gal4, *UAS egr, tub*Gal80^{ts}/+. Extended Data Fig. 6g: w^-; *UAS-traf2* RNAi GD /+; *rn*-Gal4, *UAS egr, tub*Gal80^{ts}/+. Extended Data Fig. 6h: w^-; *UAS-tak1* RNAi KK/+; *rn*-Gal4, *UAS egr, tub*Gal80^{ts}/+. Extended Data Fig. 6i: w^-; *grnd^{Minos}/ grnd^{Minos}*; *rn*-Gal4, *UAS egr, tub*Gal80^{ts}/+. Extended Data Fig. 6j: w^-; *grnd^{Minos}/ grnd^{Df}*; *rn*-Gal4, *UAS egr, tub*Gal80^{ts}/+.

Extended Data Fig. 7a: *yw, ey-FLP*; *Act>y$^+$>*Gal4, *UAS GFP*; +; *FRT82B*/ FRT82B, *tub*Gal80. Extended Data Fig. 7b: *yw, ey-FLP*; *Act>y$^+$>*Gal4, *UAS GFP*; +; *FRT82B, scrib^1*/ FRT82B, *tub*Gal80. Extended Data Fig. 7c: *yw, ey-FLP*; *Act>y$^+$>*Gal4, *UAS GFP; UAS grnd* RNAi KK /+; *FRT82B, scrib^1*/ FRT82B,

*tub*Gal80. Extended Data Fig. 7d: *ey-FLP; Act>CD2>*Gal4, *UAS GFP/ UAS grnd* RNAi KK *;* +. Extended Data Fig. 7e–g: *yw*, *ey-FLP*; *Act>y*$^{+}$>Gal4, *UAS GFP*; *UAS ras*^{V12} /+; *FRT82B, scrib*^{1}/ FRT82B, *tub*Gal80.

Extended Data Fig. 8a: *yw*, *ey-FLP*; *Act>y*$^{+}$>Gal4, *UAS GFP; UAS ras*^{V12}/+; *FRT82B, scrib*^{1}/ FRT82B, *tub*Gal80. Extended Data Fig. 8b: *yw*, *ey-FLP*; *Act>y*$^{+}$>Gal4, *UAS GFP*; *UAS ras*^{V12}, UAS *grnd* RNAi KK /+*; FRT82B, scrib*^{1}/ FRT82B, *tub*Gal80. Extended Data Fig. 8c: *yw*, *ey-FLP*; *Act>y*$^{+}$>Gal4, *UAS GFP*; *UAS ras*^{V12}, *UAS dilp8* RNAi KK /+*; FRT82B, scrib*^{1}/ FRT82B, *tub*Gal80. Extended Data Fig. 8d: *w; UAS ras*^{V12}*, UAS-dlg RNAi GD* /+*; ey-FLP*; *Act*≫Gal4, *UAS GFP* /+. Extended Data Fig. 8e: *w; UAS ras*^{V12}*, UAS-dlg RNAi GD / UAS-grnd* RNAi GD *; ey-FLP*; *Act*≫Gal4, *UAS GFP* /+. Extended Data Fig. 8f: *w; UAS ras*^{V12}*, UAS-dlg RNAi GD / UAS-grnd* RNAi KK *; ey-FLP*; *Act*≫Gal4, *UAS GFP* /+. Extended Data Fig. 8g: *wgn*^{KO}*; UAS ras*^{V12}*, UAS-dlg RNAi GD* /+*; ey-FLP*; *Act*≫Gal4, *UAS GFP* /+.

Extended Data Fig. 9a: *w*$^{-}$*;* +*;* +*; rn*-Gal4, *UAS avl* RNAi GD/+. Extended Data Fig. 9b: *w*$^{-}$*; egr*^{1} */ egr*^{3} *; rn*-Gal4, *UAS avl* RNAi GD/+. Extended Data Fig. 9c, d: *w*$^{-}$*;* +*;* +. Extended Data Fig. 9e: *w*$^{-}$*; elav*-Gal80/+*; rn*-Gal4, *UAS avl* RNAi GD/ +. Extended Data Fig. 9f: *w*$^{-}$*; UAS crb-intra/*+*; rn*-Gal4 /+. Extended Data Fig. 9g: *w*$^{-}$*; elav*-Gal80/+*; rn*-Gal4, *UAS avl* RNAi GD/+. Extended Data Fig. 9h: *w*$^{-}$*; UAS crb-intra/*+*; rn*-Gal4 /+. Extended Data Fig. 9i: *wgn*^{KO}*; UAS crb-intra/*+*; rn*-Gal4 /+. Extended Data Fig. 9j: *w*$^{-}$*;* +*; rn*-Gal4 */ diap-GFP*. Extended Data Fig. 9k: *w*$^{-}$*; UAS crb-intra/*+*; rn*-Gal4 */ diap-GFP*. Extended Data Fig. 9l: *w*$^{-}$*; UAS crb-intra/ UAS-grnd* RNAi KK *; rn*-Gal4 */ diap-GFP*.

Extended Data Fig. 10f, g: *yw, hsFLP;* +*; FRT82B, Ubi-GFP/ FRT82B, crb*^{11A22}. Extended Data Fig. 10h: *yw, hs-FLP; Act>CD2>Gal4, UAS GFP / UAS veli* RNAi *; UAS veli* RNAi /+.

27. Geuking, P., Narasimamurthy, R. & Basler, K. A genetic screen targeting the tumor necrosis factor/Eiger signaling pathway: identification of *Drosophila* TAB2 as a functionally conserved component. *Genetics* **171,** 1683–1694 (2005).
28. Izaddoost, S., Nam, S. C., Bhat, M. A., Bellen, H. J. & Choi, K. W. *Drosophila* Crumbs is a positional cue in photoreceptor adherens junctions and rhabdomeres. *Nature* **416,** 178–183 (2002).
29. Zhang, L. *et al.* The TEAD/TEF family of transcription factor Scalloped mediates Hippo signaling in organ size control. *Dev. Cell* **14,** 377–387 (2008).
30. Martín-Blanco, E. *et al. puckered* encodes a phosphatase that mediates a feedback loop regulating JNK activity during dorsal closure in *Drosophila*. *Genes Dev.* **12,** 557–570 (1998).
31. Rong, Y. S. *et al.* Targeted mutagenesis by homologous recombination in *D. melanogaster*. *Genes Dev.* **16,** 1568–1581 (2002).
32. Ruel, L., Rodriguez, R., Gallet, A., Lavenant-Staccini, L. & Therond, P. P. Stability and association of Smoothened, Costal2 and Fused with Cubitus interruptus are regulated by Hedgehog. *Nature Cell Biol.* **5,** 907–913 (2003).
33. Ciccarelli, F. D. *et al.* Toward automatic reconstruction of a highly resolved tree of life. *Science* **311,** 1283–1287 (2006).

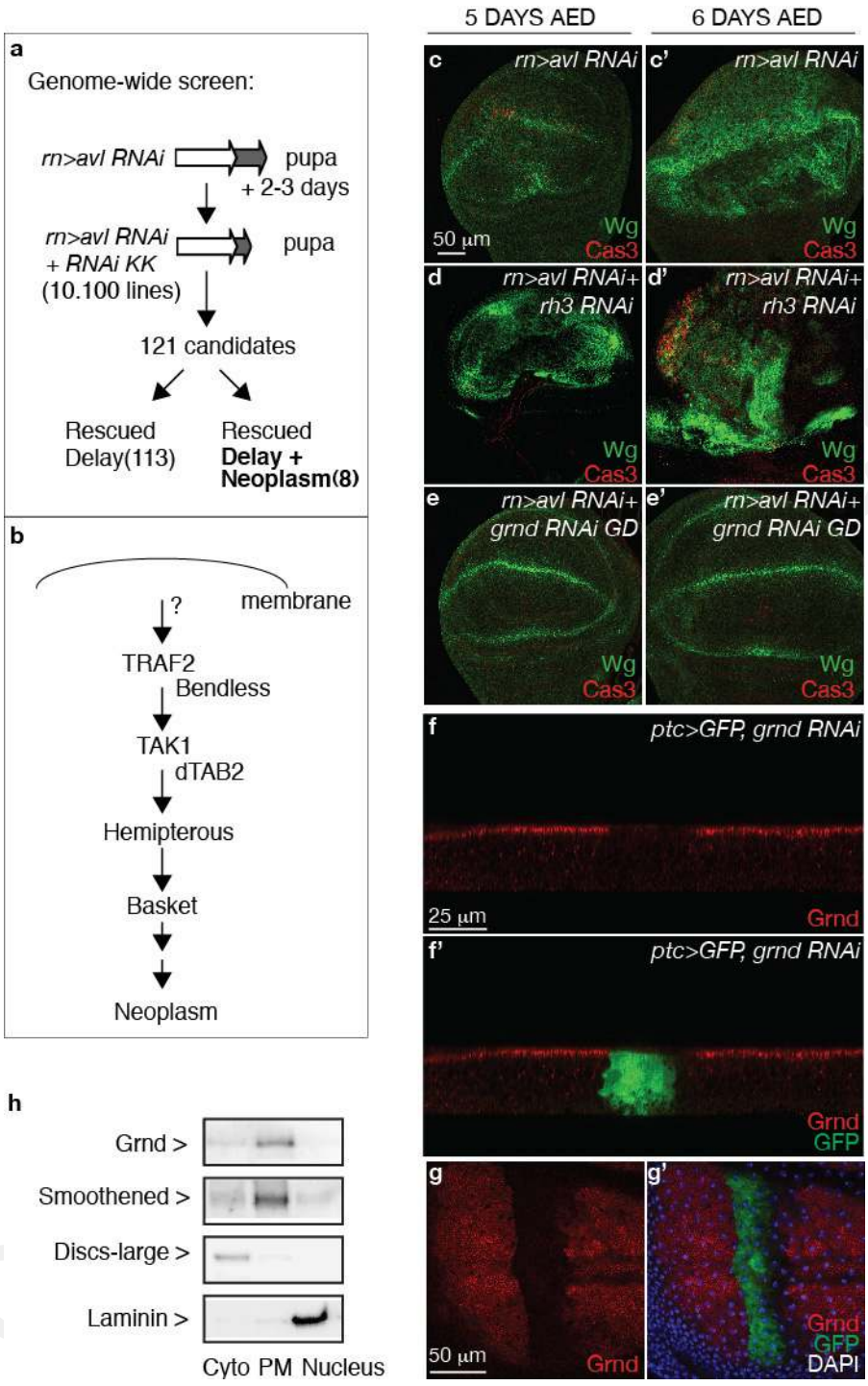

Extended Data Figure 1 | Identification of Grnd in a genetic screen for molecules implicated in neoplastic growth. **a**, Schematic of the genome-wide screen. Ten-thousand one-hundred RNAi lines were screened for their abilities to rescue the delay of the *rn>avl*-RNAi condition. Of the 121 candidates able to rescue the delay of the *rn>avl* condition, only 8 also rescued the neoplastic growth. **b**, Schematic of the five components of the JNK pathway shown to be required for the neoplastic overgrowth in the *avl* loss of function condition. Although no RNAi line targeting Traf2 was included in the original screen, Traf2 was subsequently shown to be required for neoplastic overgrowth in the *avl*-RNAi condition using an alternative RNAi line. **c–e,** Wing discs of the indicated genotypes dissected 5 days (left) or 6 days (right) AED and stained for Wg (green) and Caspase3 (red). **f, g**, Transverse (**f**) or *xy* (**g**) sections of dissected wing discs expressing *grnd* RNAi in the patch domain (GFP, green) stained for Grnd (red) and DAPI (**g**, right, blue) to visualize the nuclei. **h**, Subcellular fractionation of cleared extract from dissected wing discs shows that Grnd, like the transmembrane receptor Smoothened, localizes to the membrane fraction (PM), whereas Disc-large remains in the cytoplasmic fraction (Cyto). Laminin serves as a control for nuclear fractions.

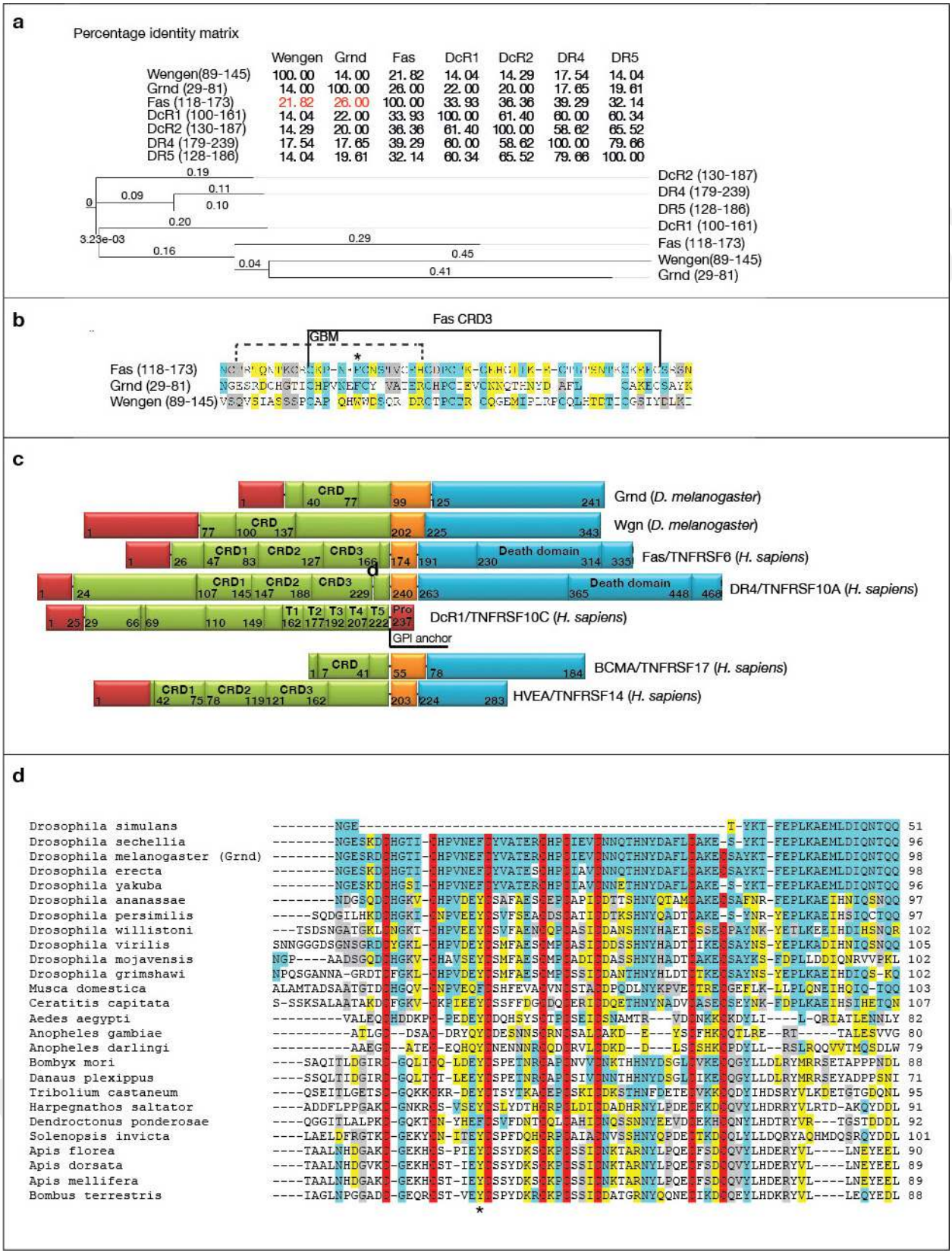
a
Percentage identity matrix
Wengen Grnd Fas DcR1 DcR2 DR4 DR5
Wengen(89-145) 100.00 14.00 21.82 14.04 14.29 17.54 14.04
Grnd (29-81) 14.00 100.00 26.00 22.00 20.00 17.65 19.61
Fas (118-173) 21.82 26.00 100.00 33.93 36.36 39.29 32.14
DcR1 (100-161) 14.04 22.00 33.93 100.00 61.40 60.00 60.34
DcR2 (130-187) 14.29 20.00 36.36 61.40 100.00 58.62 65.52
DR4 (179-239) 17.54 17.65 39.29 60.00 58.62 100.00 79.66
DR5 (128-186) 14.04 19.61 32.14 60.34 65.52 79.66 100.00
0.19
0.11
0.09
0
0.10
0.20
3.23e-03
0.29
0.16
0.45
0.04
0.41
DcR2 (130-187)
DR4 (179-239)
DR5 (128-186)
DcR1 (100-161)
Fas (118-173)
Wengen(89-145)
Grnd (29-81)
b
Fas CRD3
GBM
Fas (118-173)
Grnd (29-81)
Wengen (89-145)
c
CRD
Grnd (D. melanogaster)
Wgn (D. melanogaster)
CRD1
CRD2
CRD3
Death domain
Fas/TNFRSF6 (H. sapiens)
DR4/TNFRSF10A (H. sapiens)
T1
T2
T3
T4
T5
Pro
DcR1/TNFRSF10C (H. sapiens)
GPI anchor
BCMA/TNFRSF17 (H. sapiens)
HVEA/TNFRSF14 (H. sapiens)
d
Drosophila simulans
Drosophila sechellia
Drosophila melanogaster (Grnd)
Drosophila erecta
Drosophila yakuba
Drosophila ananassae
Drosophila persimilis
Drosophila willistoni
Drosophila virilis
Drosophila mojavensis
Drosophila grimshawi
Musca domestica
Ceratitis capitata
Aedes aegypti
Anopheles gambiae
Anopheles darlingi
Bombyx mori
Danaus plexippus
Tribolium castaneum
Harpegnathos saltator
Dendroctonus ponderosae
Solenopsis invicta
Apis florea
Apis dorsata
Apis mellifera
Bombus terrestris

Extended Data Figure 2 | Sequence homology of the extracellular domain of Grnd to CRDs of human TNFRs. **a**, Per cent identity matrix and phylogenic data from multiple local sequence alignment of the entire extracellular domains of Grnd and Wgn with extracellular domains (corresponding to a part of CRD2 and all of CRD3) of various human TNFR superfamily members. The extracellular domain of Grnd shares the highest identity with the GBM-harbouring CRD of Fas (26%). A similar result is observed for Wgn, although it exhibits lower identity (22%) and a higher degree of divergence to Fas. **b**, Sequence alignment of Fas, Grnd and Wgn demonstrates that Grnd shares a higher degree of similarity with the GBM-harbouring CRD of Fas than Wgn. This is particularly apparent in the immediate region encompassing the functionally critical F134 (marked with an asterisk) of the GBM of Fas. Blue indicates residue identity, yellow strong similarity, and grey weak similarity of Fas with Grnd and/or Wgn. **c**, Schematic representation of Grnd, Wgn, and various members of the human TNFR superfamily showing a high level of diversity in the number and arrangement of CRDs. The colour codes used are: red for signal peptide, green for extracellular domains, orange for transmembrane domains, and blue for intracellular domain. Numbers in each box indicate corresponding amino acid positions. Pro, prodomain; T1–5, TAPE1–5 (threonine-, alanine-, proline- and glutamine-rich repeats). **d**, Multiple sequence alignment showing the conservation of the extracellular domain of Grnd in other insect species. Whereas global similarity of the extracellular domain of Grnd degenerates outside the melanogaster group, the cysteine residues of the CRD (highlighted in red) and the aromatic residue (F/Y, marked with an asterisk) corresponding to F134 of Fas CRD3 remain highly conserved throughout the Hymenoptera order. Blue indicates residue identity; yellow, strong similarity; and grey, weak similarity to Grnd.

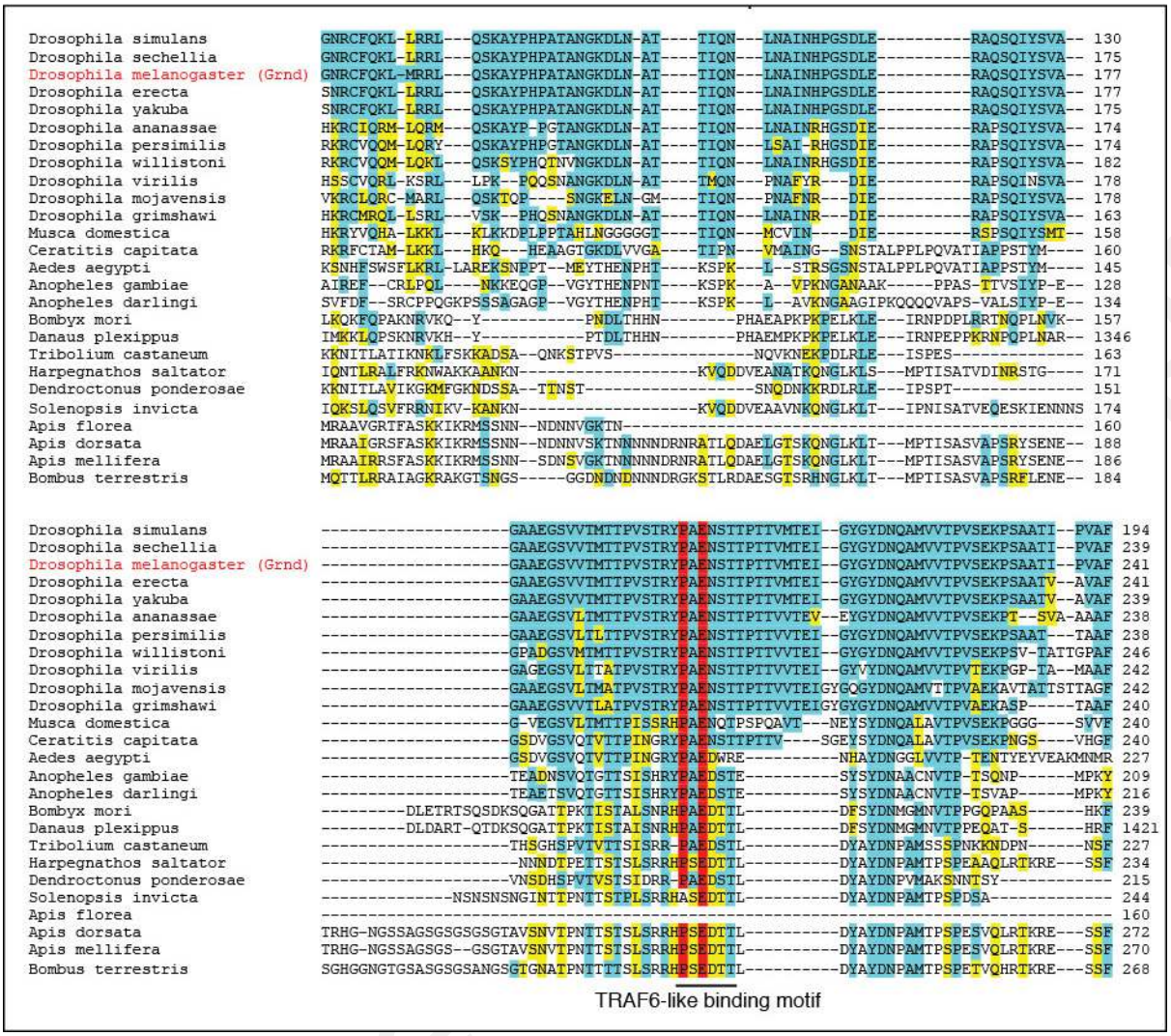

Extended Data Figure 3 | Identification of a conserved TRAF6-like binding motif in the intracellular domain of Grnd proteins. Multiple sequence alignment of the intracellular domain of Grnd and Grnd-like proteins in other species. A binding motif for TRAF6 (PxExx(aromatic/acidic residue)), the closest homologue of *Drosophila* Traf2, was previously identified in human TNFRs[4]. The position of a related putative Traf2-binding motif in the intracellular domain of Grnd is indicated. Note that, although sequence similarity of the intracellular domain of Grnd degenerates outside the family Drosophilidae, the core residues of this motif (highlighted in red) remain highly conserved throughout the order Hymenoptera. Blue indicates residue identity; yellow, strong similarity to Grnd.

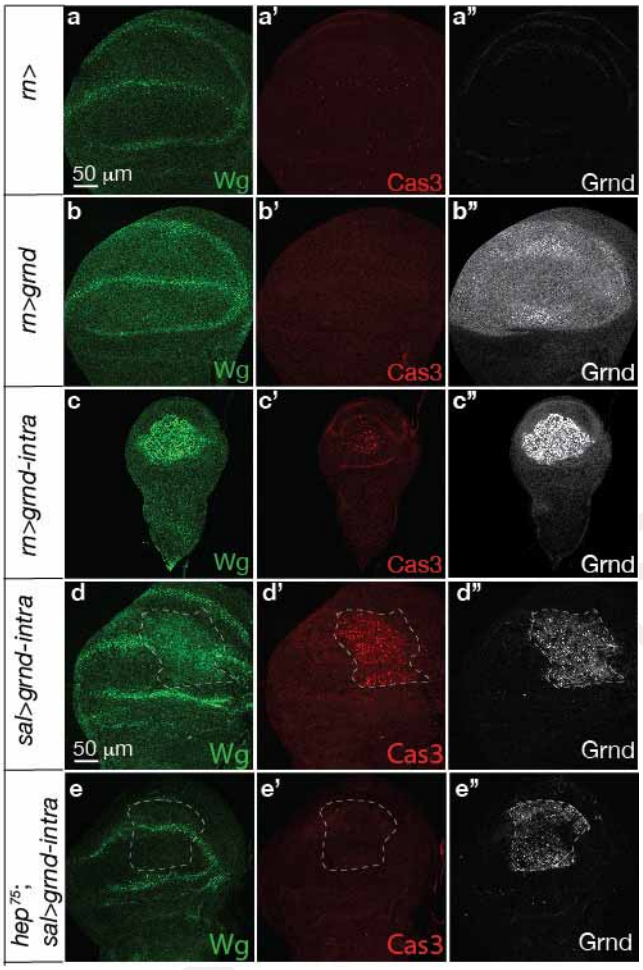

Extended Data Figure 4 | Grnd acts upstream of JNK signalling. a–d, Wild-type wing discs (**a**) or discs expressing *grnd* (**b**) or *grnd-intra* (**c, d**) in the *rn* domain were dissected 5 days AED and stained for Wg (left; green), Cas3 (middle; red), and Grnd (right; grey). **d**, **e**, Wing discs expressing *grnd-intra* in the *sal* domain (marked by a truncated line) in a wild-type (**d**) or *hep*^{75} mutant (**e**) background were dissected 5 days AED and stained for Wg (left; green), Cas3 (middle; red), and Grnd (right; grey).

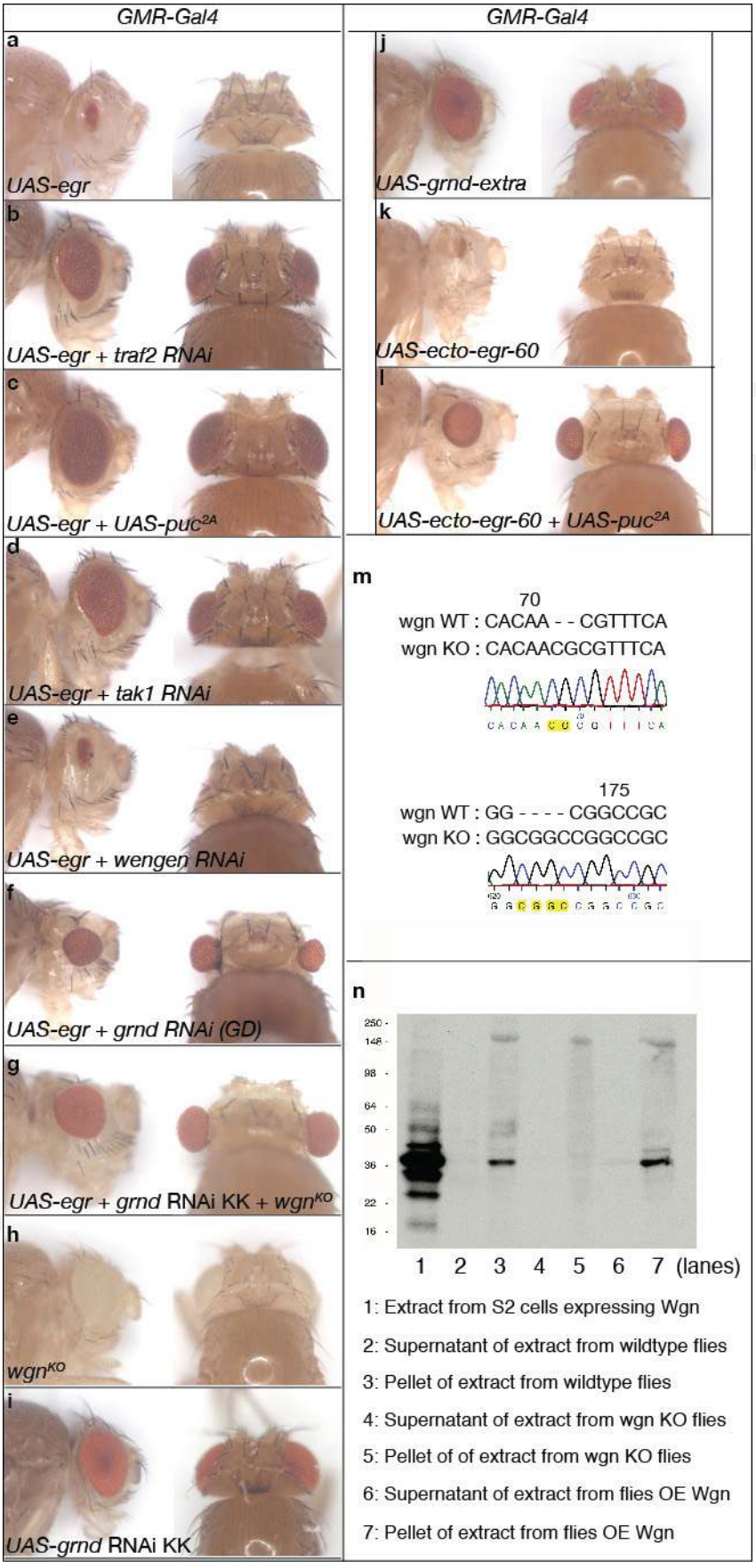

Extended Data Figure 5 | Characterization of the *wgn*^{KO} mutant allele. **a–e**, Light micrographs of *Drosophila* adult eyes are shown. Original magnification, ×30. The small-eye phenotype caused by *GMR*-driven expression of *egr* (**a**) is rescued by co-expressing *puc* (**c**) or reducing the activity of Traf2 (**b**), but not by reducing Wgn activity (**d**; also serves as a control to exclude a Gal4 titration effect). **f**, **g**, Reducing Grnd activity partially rescues the small-eye phenotype, giving rise to the hanging-eye phenotype (**f**) and is not further rescued in a *wgn*^{KO} mutant background (**g**). **h**, *wgn*^{KO} mutant flies do not display any eye phenotype. **i**, **j**, Reducing Grnd levels or expressing Grnd-extra in the *GMR* domain does not affect eye morphology. **k**, GMR-Gal4-induced expression of a soluble form of Egr lacking the transmembrane and cytoplasmic domain (Ecto-Egr-60) gives rise to a small-eye phenotype[10]. **l**, Co-expression of *puc*^{2A} in a *GMR>ecto-egr-60* background partially rescues the small-eye phenotype, giving rise to a hanging-eye phenotype[10]. **m**, Sequence analysis of DNA extracted from flies homozygous for the *wgn*^{KO} mutation showing the two frameshift mutations introduced by cutting the unique intrinsic restriction sites AclI (exon 1) and NotI (exon 2) followed by T4 DNA polymerase-mediated fill-in. **n**, Western blot of fly extracts from the indicated genotypes probed with an anti-Wgn antibody[27]. KO, knockout; OE, overexpressing; WT, wild type.

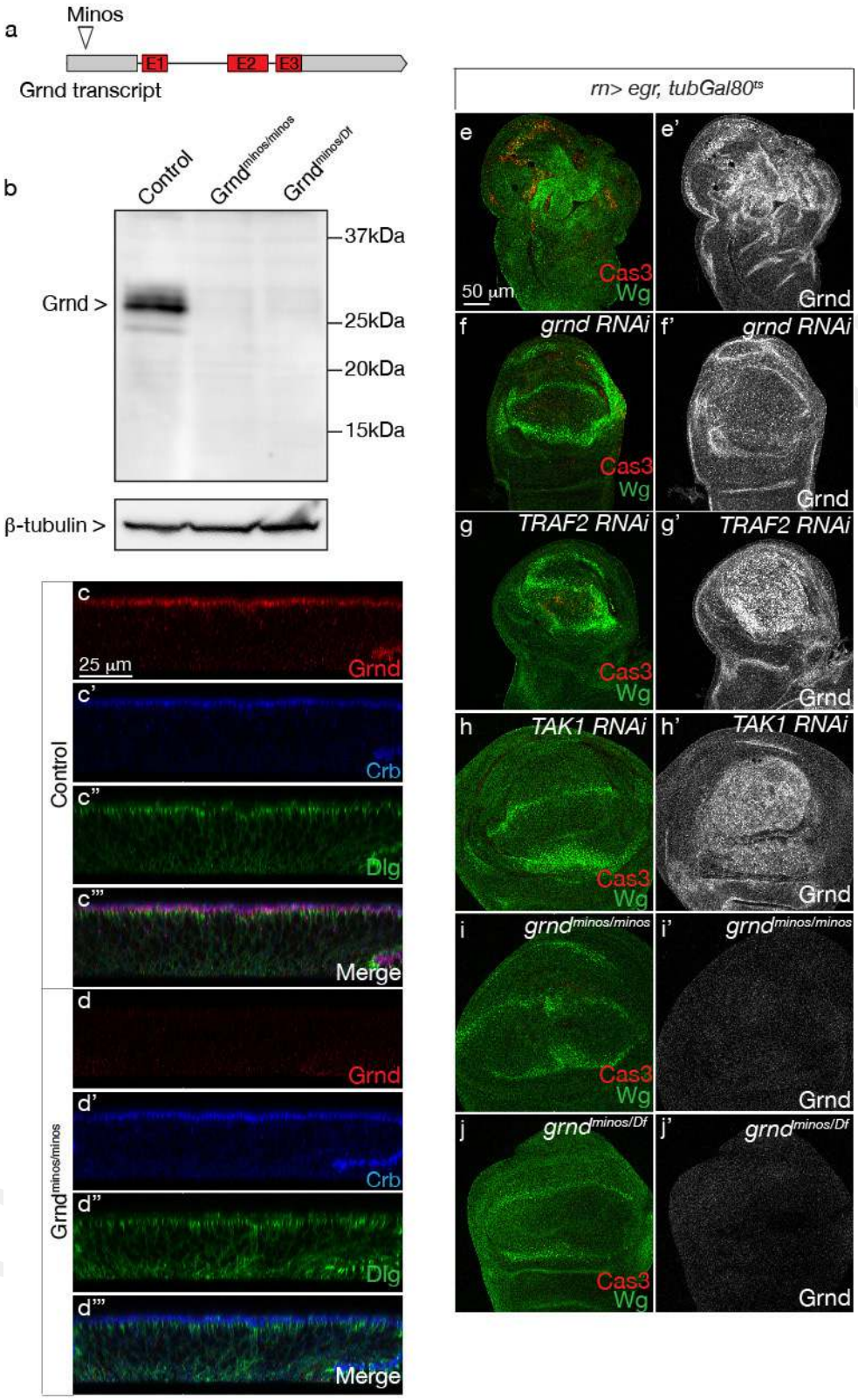

Extended Data Figure 6 | Characterization of the *grnd*^{Minos} mutant. **a**, Schematic representation of the Minos transposon insertion in the *grnd* gene region corresponding to the 5′ untranslated region of the transcript. **b**, Western blot of wing disc extracts from the indicated genotypes probed with anti-Grnd (top) and anti-β-tubulin (bottom) antibodies. Grnd protein migrates at the predicted size of 27 kDa (lane 1, control). Grnd protein levels are decreased below detection level in both *grnd*$^{Minos/Minos}$ and *grnd*$^{Minos/Df}$ mutant flies, indicating that *grnd*$^{Minos/Minos}$ is indistinguishable from a null mutant. **c**, **d**, Polarity is not affected in *grnd*$^{Minos/Minos}$ and *grnd*$^{Minos/Df}$ wing discs. Transverse sections of dissected control (**c**) or *grnd*$^{Minos/Minos}$ (**d**) wing discs stained for Grnd (top; red), Crb (middle top; blue) and Dlg (middle bottom; green). **e–j**, Wing discs dissected from third instar larvae after 40 h of Egr expression in the *rn* domain. Pouch ablation, ubiquitous Wg expression and apoptosis observed in *rn>egr, Tub*-Gal80^{ts} discs (**e**) are suppressed to various extents upon co-expression of *grnd*-RNAi (**f**) or reduction of JNK activity (**g**, **h**) and fully suppressed in *grnd*$^{Minos/Minos}$ (**i**) and *grnd*$^{Minos/Df}$ (**j**) mutant backgrounds.

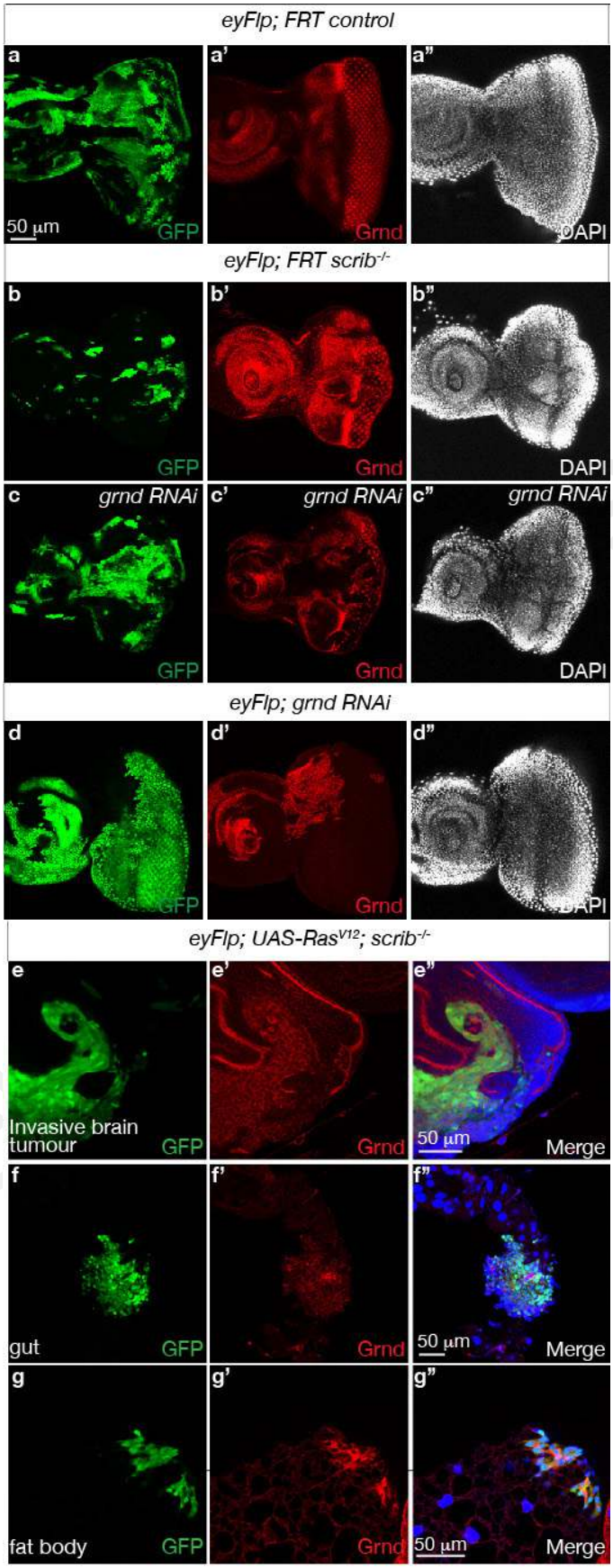

Extended Data Figure 7 | Grnd is highly expressed in *Ras^{V12}/scrib$^{-/-}$* micro-metastases. **a–c,** Reducing *grnd* levels in *scrib$^{-/-}$* mutant clones prevent their elimination. Eye discs dissected 5 days AED carrying GFP-labelled MARCM clones of the indicated genotypes stained for Grnd (middle; red) and DAPI (right; grey). **d,** Reducing Grnd levels does not affect cell viability. Eye discs dissected 5 days AED carrying GFP-labelled *grnd* RNAi Flip-out clones stained for Grnd (middle; red) and DAPI (right; grey). **e–g,** Invasive brain tumours and micro-metastases display high levels of Grnd protein. Dissected eye–brain complex (**e**), gut (**f**) and fat body (**g**) displaying GFP-labelled invasive *Ras^{V12}/scrib$^{-/-}$* clones (**e**; green) or micro-metastases (**f**, **g**; green) stained for Grnd (red) and DAPI (blue).

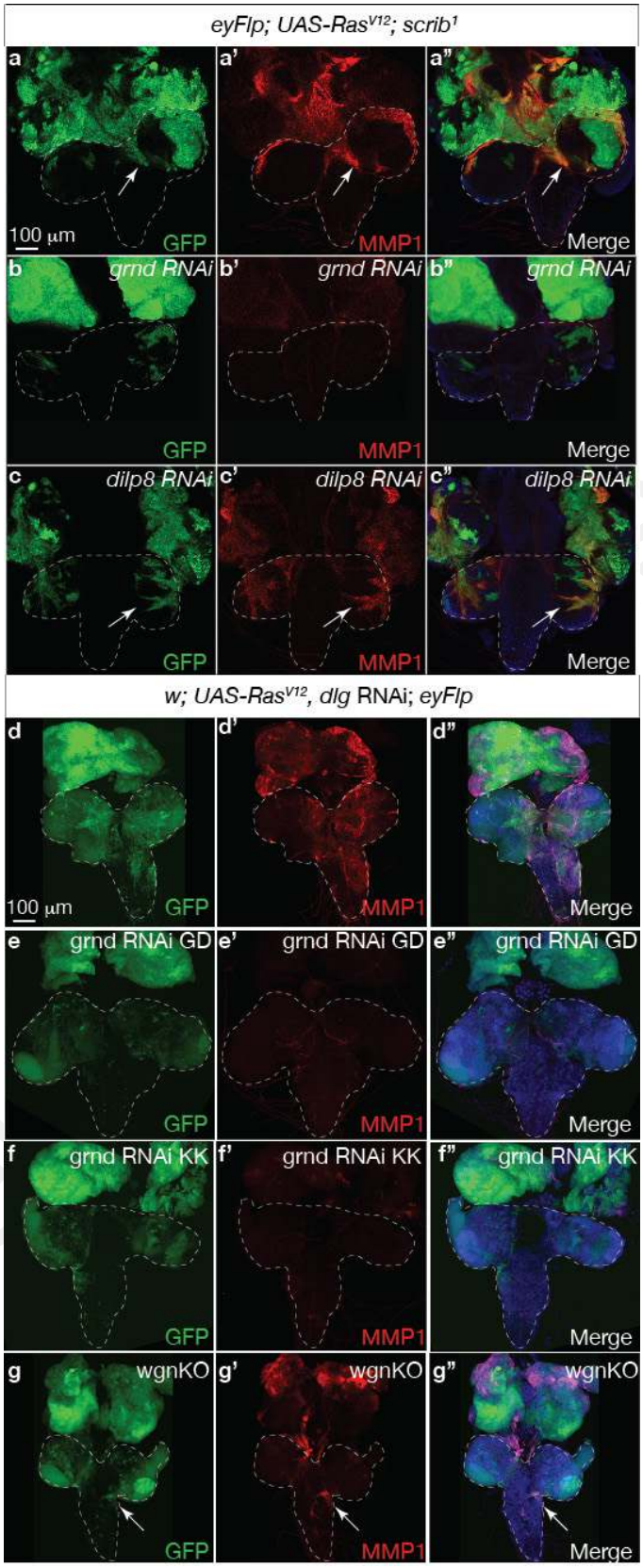

Extended Data Figure 8 | Grnd, but not Wgn, is required for Mmp1 expression both in *Ras^{V12}/scrib^{1}* and *Ras^{V12}/Dlg* RNAi tumours. a–c, Eye–brain complexes dissected 7 days AED carrying *Ras^{V12}/scrib$^{-/-}$* (**a**), *Ras^{V12}/scrib$^{-/-}$* + *grnd*-RNAi (**b**), or *Ras^{V12}/scrib$^{-/-}$* + *dilp8*-RNAi (**c**; control RNAi to exclude a Gal4 titration effect) clones labelled by GFP and stained for Mmp1 (middle; red). *Ras^{V12}/scrib$^{-/-}$* and *Ras^{V12}/scrib$^{-/-}$* + *dilp8*-RNAi clones invade the ventral nerve cord (**a**, **c**; see white arrow). **d–g,** Eye–brain complexes dissected 7 days AED carrying *Ras^{V12}/Dlg*-RNAi (**d**) or *Ras^{V12}/Dlg*-RNAi + *grnd*-RNAi (**e, f**) clones (labelled by GFP), or *Ras^{V12}/Dlg*-RNAi GFP-labelled clones in a *wgn*-null mutant background (**g**) stained for Mmp1 (middle; red) and DAPI (right; blue). *Ras^{V12}/Dlg* RNAi clones invade the ventral nerve cord in *wgn*-null mutant animals (**g**; see white arrow).

avl RNAi-induced neoplastic growth.",5,1,0,0,600pt,600pt,0pt,0pt >

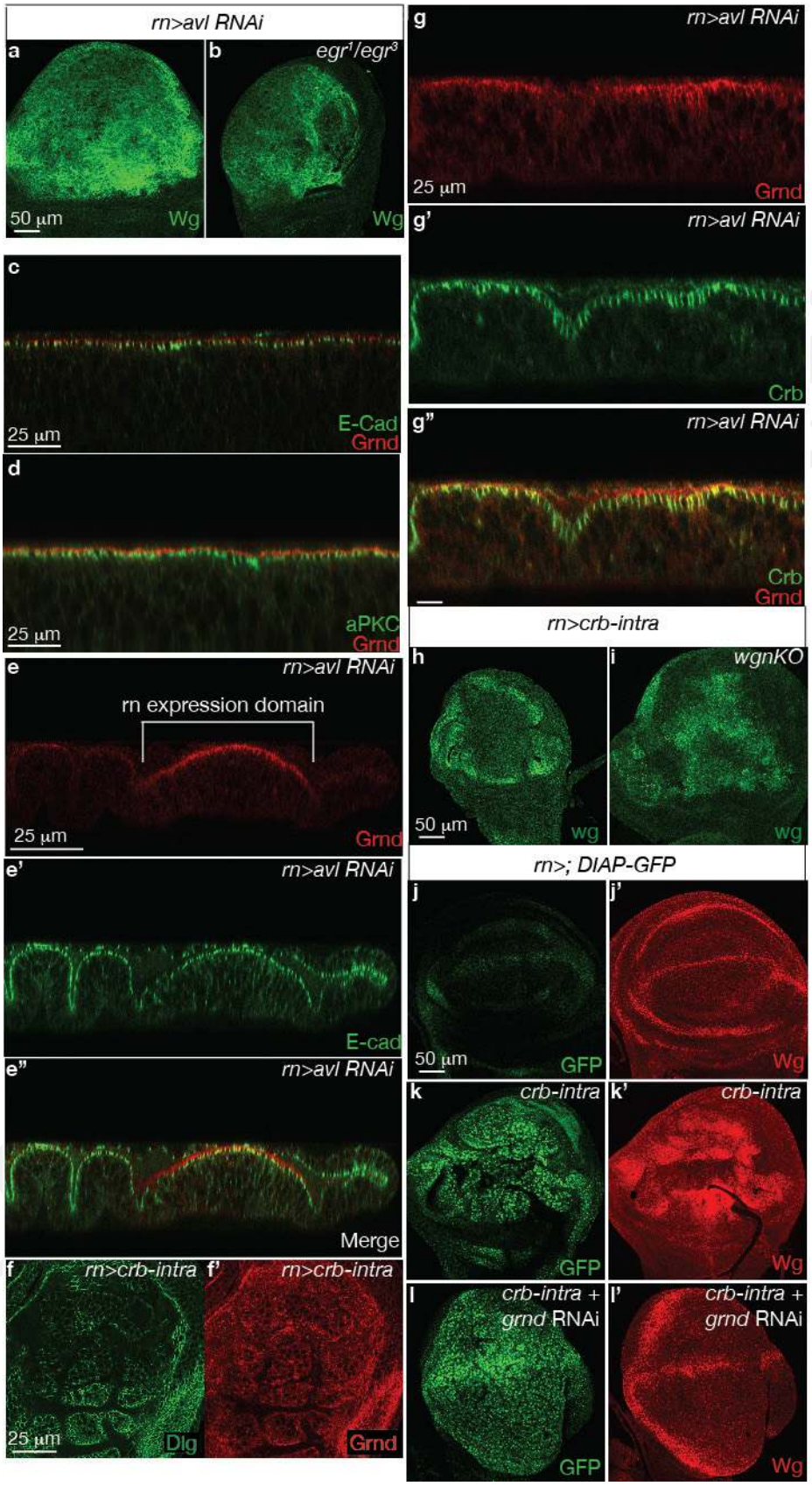

Extended Data Figure 9 | Egr is not required for the *rn>avl* RNAi-induced neoplastic growth. a, b, Wing discs of the indicated genotypes dissected 6 days AED and stained for Wg (green). **c, d**, Transverse sections of dissected wild-type discs stained for Grnd (red) and either E-cad (**c**; in green), or aPKC (**d**; in green). **e**, **g**, Transverse sections of *rn>avl* RNAi wing discs dissected 5 days AED and stained for Grnd (top, bottom; red) and either E-cad (**e**, middle, bottom; green) or Crb (**g**, middle, bottom; green). The *rn* expression domain is indicated (**e**, top). **f**, Wing discs expressing *crb-intra* in the *rn* domain (*rn>crb-intra*) dissected 6 days AED and stained for Disc-large (Dlg, green) to visualize neoplastic structures and Grnd (red). **h**, **i**, Wing discs expressing *crb-intra* in the *rn* domain of wild-type (**h**) or *wgn*-knockout mutant (**i**) animals dissected 6 days AED and stained for Wg (green). **j–l**, Reducing *grnd* levels does not affect *crb-intra*-mediated inhibition of Hippo signalling, which causes an upregulation of the Yki transcriptional target Diap1. Control discs (**j**) or wing discs expressing Crb-intra alone (**k**) or together with *grnd* RNAi (**l**) in the *rn* domain were dissected from animals carrying a reporter gene for Hippo pathway activity (*Diap-GFP*, green) and stained for Wg (red).

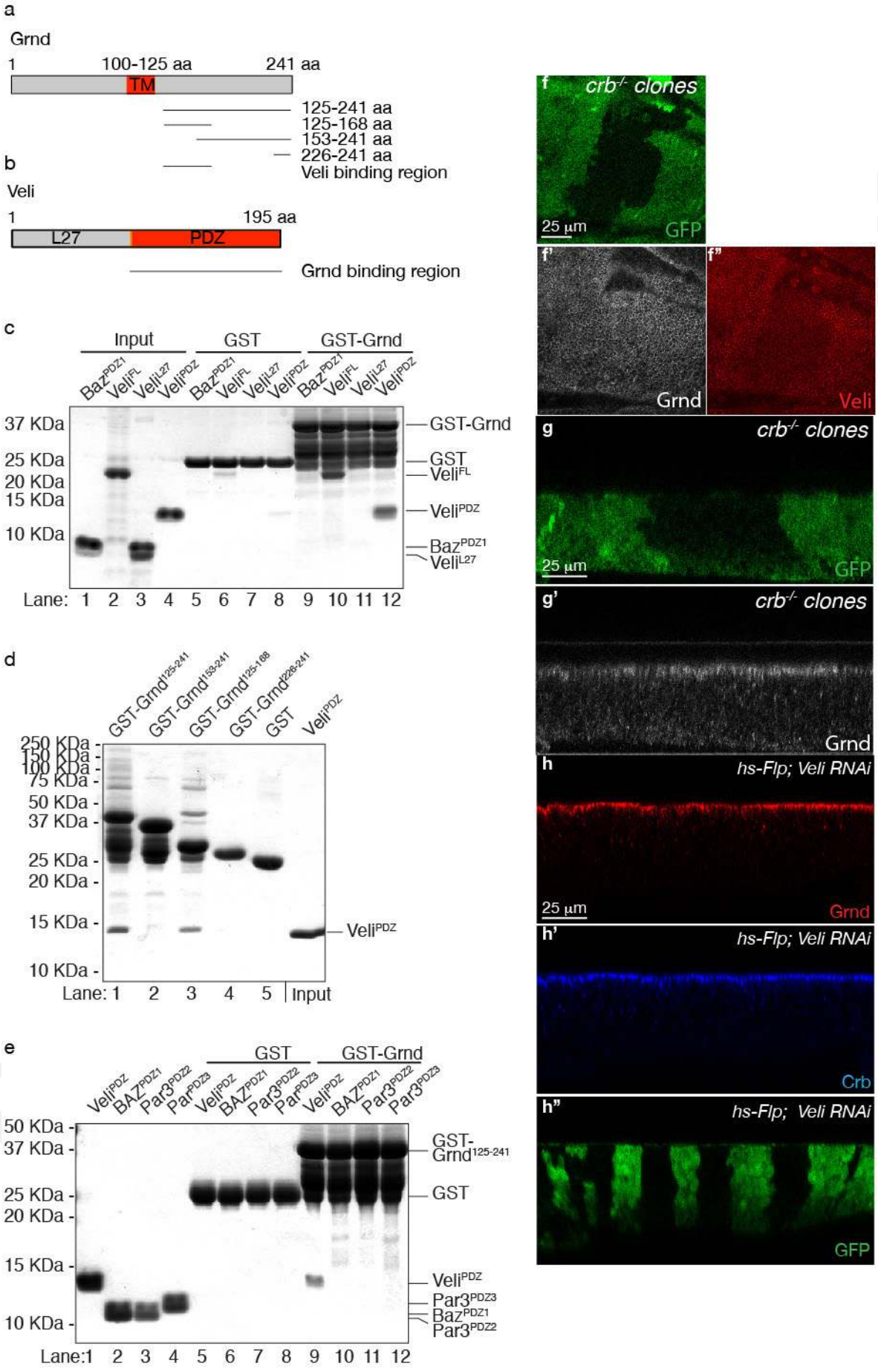
a
Grnd
1
100-125 aa
241 aa
TM
125-241 aa
125-168 aa
153-241 aa
226-241 aa
Veli binding region
b
Veli
1
195 aa
L27
PDZ
Grnd binding region
c
Input
GST
GST-Grnd
BazPDZ1
VeliFL
VeliL27
VeliPDZ
37 KDa
25 KDa
20 KDa
15 KDa
10 KDa
GST-Grnd
GST
VeliFL
VeliPDZ
BazPDZ1
VeliL27
Lane: 1 2 3 4 5 6 7 8 9 10 11 12
d
GST-Grnd125-241
GST-Grnd153-241
GST-Grnd125-168
GST-Grnd226-241
GST
VeliPDZ
250 KDa
150 KDa
100 KDa
75 KDa
50 KDa
37 KDa
25 KDa
20 KDa
15 KDa
10 KDa
VeliPDZ
Lane: 1 2 3 4 5 Input
e
GST
GST-Grnd
VeliPDZ
BAZPDZ1
Par3PDZ2
Par3PDZ3
50 KDa
37 KDa
25 KDa
20 KDa
15 KDa
10 KDa
GST-Grnd125-241
GST
VeliPDZ
Par3PDZ3
BazPDZ1
Par3PDZ2
Lane:1 2 3 4 5 6 7 8 9 10 11 12
f
crb-/- clones
25 µm
GFP
f'
Grnd
f"
Veli
g
crb-/- clones
25 µm
GFP
g'
crb-/- clones
Grnd
h
hs-Flp; Veli RNAi
25 µm
Grnd
h'
hs-Flp; Veli RNAi
Crb
h"
hs-Flp; Veli RNAi
GFP

Extended Data Figure 10 | Grnd directly interacts with the PDZ domain of Veli and neither depends on Veli nor Crb for its proper localization. a, b, Schematic representation of Grnd and Veli (also known as Lin-7) domains and the various truncations used to map the interface of the Grnd–Veli interaction. L27, Lin-2/Lin-7 domain; PDZ, PSD-95/Dlg/ZO-1 domain; TM, transmembrane domain. **c**, GST–Grnd$^{125–241}$ immobilized on GSH beads was incubated with full-length Veli (Veli^{FL}) or the complementary Veli fragments L27 (Veli^{L27}) and PDZ domain (Veli^{PDZ}). The PDZ1 domain of the polarity protein Bazooka was included in the pull-down as a specificity control (Baz^{PDZ1}). Coomassie-blue stained SDS–polyacrylamide gel electrophoresis (SDS–PAGE) was used to visualize species retained on beads. Veli^{FL} and Veli^{PDZ} bind to Grnd (lanes 10 and 12), but not Veli^{L27} nor Baz^{PDZ1} (lanes 11 and 9), indicating that Grnd specifically recognizes the PDZ domain of Veli. **d**, To map the interface between Grnd and Veli^{PDZ}, the same binding assay was performed using a battery of Grnd deletion mutants adsorbed on GSH beads. Veli^{PDZ} forms a complex with Grnd$^{125–241}$ and Grnd$^{125–168}$ (lanes 1 and 3), but not with the carboxy-terminal region of Grnd (lanes 2 and 4) or GST alone (lane 5, control). **e**, To address further the specificity of the binding of Grnd$^{125–241}$ to the PDZ domain of Veli, we repeated the pull-down assay with the PDZ domains of Baz and its human orthologue PAR3. Veli^{PDZ} is retained on GST–Grnd$^{125–241}$ beads (lane 9), while PAR3^{PDZ2}, PAR3^{PDZ3} and Baz^{PDZ1} are not (lanes 10, 11 and 12). **f–g**, Reducing Crb levels affects the localization of Veli, but not Grnd. **f–g**, *xy* (**f**) or transverse (**g**) sections of dissected wing discs bearing *crb*$^{-/-}$ mutant clones (labelled by absence of GFP) stained for Grnd (**f**, bottom left, **g**, bottom; white) or Veli (**f**, bottom right; red). **h**, Reducing Veli levels does not affect Crb[20] or Grnd localization. Transverse sections of dissected wing discs bearing clones expressing *veli* RNAi (**h**, bottom; labelled by the presence of GFP) stained for Grnd (top; red) and Crb (middle; blue).